X-linked intellectual disability mutations alter the conformational state of a histone demethylase's sensing of chromatin

Fatima S. Ugur[1,3], Mark J. S. Kelly[2], and Danica Galonić Fujimori[2,3,4*]

[1] Chemistry and Chemical Biology Graduate Program, [2] Department of Pharmaceutical Chemistry, [3] Department of Cellular and Molecular Pharmacology, [4] Quantitative Biosciences Institute, University of California, San Francisco, San Francisco, CA

*To whom correspondence should be addressed: danica.fujimori@ucsf.edu

Running title: Altered sensing of chromatin by KDM5C in XLID

Keywords: histone demethylase, histone methylation, nucleosome, chromatin, intellectual disability, missense mutation, chromatin regulation, protein conformation

ABSTRACT

The H3K4me3 chromatin modification, a hallmark of promoters of actively transcribed genes, is dynamically removed by the KDM5 family of histone demethylases. The KDM5 demethylases have a number of accessory domains, two of which, ARID and PHD1, lie within the catalytic domain. KDM5C, which has a unique role in neural development, harbors a number of mutations adjacent to its accessory domains that cause X-linked intellectual disability (XLID). The roles of these accessory domains remain unknown, limiting an understanding of how XLID mutations affect KDM5C activity. We find that while the ARID and PHD1 domains are required for efficient nucleosome demethylation, the PHD1 domain alone has an inhibitory role in KDM5C catalysis. We further find that binding of the H3 tail to PHD1 is coupled to the recognition of linker DNA by KDM5C. Our data suggests a model in which the PHD1 domain regulates DNA recognition by the ARID domain based on available substrate cues. In this model, recognition of distinct chromatin features is coupled to a conformational rearrangement of the ARID and PHD1 domains, which in turn modulates the positioning of the catalytic domain for efficient nucleosome demethylation. Importantly, we find that XLID mutations adjacent to the ARID and PHD1 domains alter the conformational state of these domains to enhance DNA binding. This results in the loss of specificity in chromatin recognition by KDM5C and renders catalytic activity sensitive to inhibition by linker DNA. Our findings suggest a unifying model by which XLID mutations alter chromatin recognition and enable euchromatin-specific dysregulation of demethylation by KDM5C.

INTRODUCTION

The methylation of lysine 4 on histone H3 is a chromatin modification found on euchromatin, where H3K4 trimethylation (H3K4me3) is present at gene promoter regions associated with active transcription, and where H3K4 monomethylation (H3K4me1) is found at active enhancer regions (1). While H3K4me1/2 is demethylated by the KDM1/LSD family, H3K4me1/2/3 is dynamically regulated by the KDM5/JARID1 subfamily of Jumonji histone demethylases (2–7). This demethylase family harbors unique accessory domains in addition to its catalytic domain comprised of the JmjN and JmjC segments that form a composite active site for demethylation (8, 9). KDM5A (RBP2, JARID1A), KDM5B (PLU-1, JARID1B), KDM5C (SMCX, JARID1C), and KDM5D (SMCY, JARID1D) all contain an AT-rich interaction domain (ARID), C_5HC_2 zinc finger domain (ZnF), and 2-3 plant homeodomains (PHD1-3). Unique to the KDM5 family is the insertion of the ARID and PHD1 domains between the JmjN and JmjC segments of the catalytic domain, and ARID and PHD1 are required for demethylase activity *in vivo* (4, 10–12). ARID domains are DNA binding domains, and ARID of KDM5A/B has been shown to bind to GC-rich DNA (13, 14). PHD domains are H3K4me reader domains with varying specificity towards unmethylated and methylated H3K4 states (15–21). PHD1 of KDM5A/B preferentially binds the unmethylated H3 tail, and this recognition of the demethylation product allosterically stimulates demethylase activity of KDM5A *in vitro* (22–27). The exact regulatory functions of recognition by these accessory domains is not entirely clear. In addition, the ARID and PHD1 domains have not been extensively studied in KDM5C, which possesses a unique function in neural development and has nonredundant demethylase activity (2, 28).

KDM5C is ubiquitously expressed but has highest expression levels in the brain (29, 30). This demethylase is important for neural development and dendrite morphogenesis, and KDM5C knockout mice have abnormal dendritic branching and display memory defects, impaired social

behavior, and aggression (2, 28). KDM5C fine-tunes the expression of neurodevelopmental genes, as gene expression levels only change less than 2 fold upon knockout of KDM5C in mice (28, 31). KDM5C localizes to enhancers in addition to promoter regions and has been shown to also fine tune enhancer function by demethylating spurious H3K4me3 at enhancers during neuronal maturation (28, 31–33). In line with its neurodevelopmental function, a number of missense and nonsense mutations that cause X-linked intellectual disability (XLID) are found throughout KDM5C (30, 34–38). As KDM5C is located on the X-chromosome and the Y paralog KDM5D cannot compensate for its function, males with KDM5C XLID mutations are primarily affected with a range of mild to severe symptoms of limitations in cognition, memory, and adaptive behavior (29, 30, 36, 37, 39). These XLID mutations are present throughout and in between the accessory domains of KDM5C, suggesting disruption of their regulatory functions. Some functionally characterized mutations have been shown to reduce demethylase activity despite not occurring in the catalytic domains, and a select few mutations have been shown to not affect demethylase activity, disrupting a nonenzymatic function instead (2, 11, 38, 40, 41). However, exactly what consequences these XLID mutations have on KDM5C at its target regions within chromatin to affect gene expression during neural development is not fully understood.

Motivated by the presence of XLID-causing mutations near the accessory domains of KDM5C, we first sought to determine the functions of the ARID and PHD1 accessory domains in KDM5C and then evaluate whether these functions might be disrupted by XLID mutations. We approached these questions by interrogating the recognition and demethylation of nucleosomes by KDM5C, as nucleosome substrates enable extended interactions by multiple domains of the demethylase. Our findings reveal that the ARID and PHD1 domains are important for nucleosome demethylation and contribute to chromatin recognition in specific contexts. We find that PHD1 of KDM5C recognizes the H3 tail and plays an inhibitory role during catalysis. PHD1 also appears to regulate the recognition of linker DNA by KDM5C, likely through modulation of the ARID

domain. Furthermore, we find that XLID mutations near these regulatory domains cause an altered conformational state of KDM5C, disrupting interdomain interactions and enabling enhanced affinity towards nucleosomal and linker DNA. This in turn results in nonproductive chromatin binding and linker DNA mediated inhibition of demethylation. Our findings establish a unique regulation of demethylase activity in KDM5C that allows for plasticity of H3K4me3 demethylation which is disrupted in X-linked intellectual disability.

RESULTS

ARID & PHD1 domain region contributes to productive demethylation but not binding of nucleosomes

Previous work has demonstrated that KDM5C is capable of demethylating H3K4me3 peptides and that the catalytic JmjN-JmjC domain and zinc finger domain are necessary for demethylase activity (2, 8, 41). To evaluate the contributions of the ARID and PHD1 domains, we sought to interrogate the recognition and demethylation of nucleosomes, given the expected interactions of these domains with DNA and histone tails, respectively. We utilized an N-terminal fragment of KDM5C containing the residues 1 to 839 necessary to observe demethylation *in vitro* ($KDM5C^{1-839}$), as well as an analogous construct where the ARID and PHD1 region (residues 83 to 378) is replaced by a linker ($KDM5C^{1-839}$ ΔAP) (Figure 1A) (8). We measured affinities of these constructs to both unmodified and substrate H3K4me3 core nucleosomes containing 147 bp DNA by electrophoretic mobility shift assay. KDM5C binds nucleosomes with weak affinity and with two fold specificity towards substrate nucleosomes, with K_d^{app} of ~8 μM for the H3K4me3 nucleosome and ~15 μM for the unmodified nucleosome (Figure 1B). Surprisingly, the ARID and PHD1 domains have a modest contribution to nucleosome binding, as $KDM5C^{1-839}$ ΔAP displays only a 2 fold reduction in nucleosome affinity and retains the two fold specificity towards the substrate

nucleosome (Figure 1B). Thus, nucleosome affinity is largely driven by H3K4me3 tail recognition by the catalytic domains in KDM5C. The absence of a significant enhancement of nucleosome binding through ARID and PHD1 domain mediated multivalent interactions suggest a more complex role of these domains rather than simply facilitating chromatin recruitment.

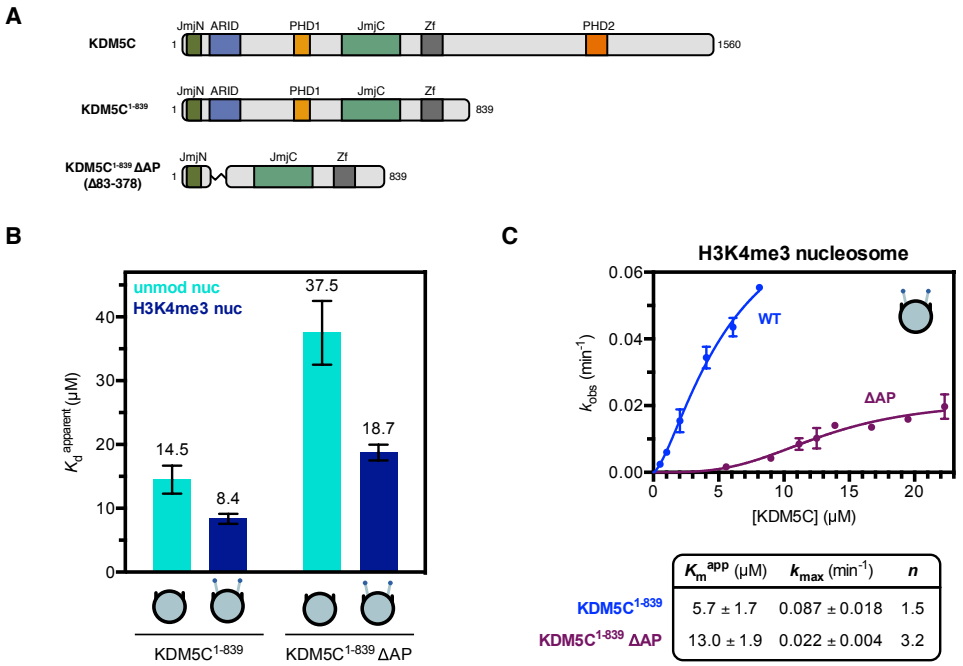

Figure 1. The ARID & PHD1 region of KDM5C contributes to efficient demethylation but not binding of nucleosomes.
(A) Domain architecture of KDM5C and KDM5C constructs used in this study. **(B)** Unmodified and substrate nucleosome binding by KDM5C constructs with apparent dissociation constants (K_d^{app}) measured by EMSA (binding curves in Figure S1B). **(C)** Demethylation kinetics of the H3K4me3 substrate nucleosome by KDM5C constructs under single turnover conditions. Observed rates are fit to a cooperative kinetic model, with *n* denoting the Hill coefficient. Representative kinetic traces used to determine observed demethylation rates are in Figure S1C. All error bars represent SEM of at least two independent experiments ($n \geq 2$).

We next interrogated the demethylase activity of KDM5C towards the H3K4me3 substrate nucleosome *in vitro* by utilizing a TR-FRET based kinetic assay that detects formation of the H3K4me1/2 product nucleosome. In order to measure true catalytic rates, demethylation was performed under single turnover conditions with enzyme in excess (42). We find that KDM5C$^{1-839}$ demethylates the substrate nucleosome with an observed catalytic rate of ~0.09 min^{-1} and KDM5C$^{1-839}$ ΔAP with a 4 fold lower catalytic rate of ~0.02 min^{-1} (Figure 1C), indicating that the

ARID and PHD1 region contributes to productive catalysis on nucleosomes, but not significantly towards nucleosome affinity. The contribution of the ARID and PHD1 domain region towards efficient demethylation appears to be through interactions of these domains with the nucleosome, as the catalytic efficiency of KDM5C$^{1-839}$ ΔAP relative to wild type is only 3 fold lower on the substrate H3K4me3 peptide, as opposed to the 9 fold reduction in catalytic efficiency on the substrate nucleosome (Figure S1A). Interactions of the ARID and PHD1 domains with the nucleosome during catalysis might better orient the catalytic domains for demethylation and could make the substrate H3K4me3 more accessible through disrupting histone tail-DNA interactions (43–46). As the ARID and PHD1 domains are poorly functionally characterized in KDM5C, we sought to next investigate the features of the nucleosome that they recognize.

PHD1 domain has an inhibitory role in KDM5C catalysis

The PHD1 domain of KDM5C has been previously shown to bind to H3K9me3 through peptide pull down (2). To interrogate the histone binding and specificity of PHD1, we purified the PHD1 domain and quantified binding to histone peptides by nuclear magnetic resonance (NMR) spectroscopy and bio-layer interferometry. We observe near identical binding between H3 and H3K9me3 tail peptides, indicating no specific binding of PHD1 towards the H3K9me3 modification (Figure S2A). Furthermore, we observe biphasic binding kinetics of PHD1 binding the H3 tail peptide, indicative of a two step binding mechanism where H3 tail binding likely induces a conformational change in PHD1 (Figure S2B). Indeed, we observe large chemical shifts of a majority of assigned residues in PHD1 upon titration of the H3 tail peptide by NMR, supportive of a conformational change in PHD1 upon binding (Figure 2A, Figure S2C). The observed affinity of PHD1 towards the H3 tail is surprisingly weak with a dissociation constant of 130 μM, about 100 fold weaker than the affinity of the homologous PHD1 of KDM5A towards the H3 tail (Figure 2B) (24, 27). However, PHD1 of KDM5C retains the same specificity towards the unmodified H3 tail

over H3K4 methylated tail peptides as observed in the PHD1 domains of KDM5A/B (Figure 2B). Interestingly, the induced conformational change in PHD1 upon H3 tail binding is linked to its methylation specificity, as chemical shifts in PHD1 decrease upon binding as the methylation state of H3K4 is increased (Figure 2B). This suggests a conformational coupling of the PHD1 domain with ligand recognition.

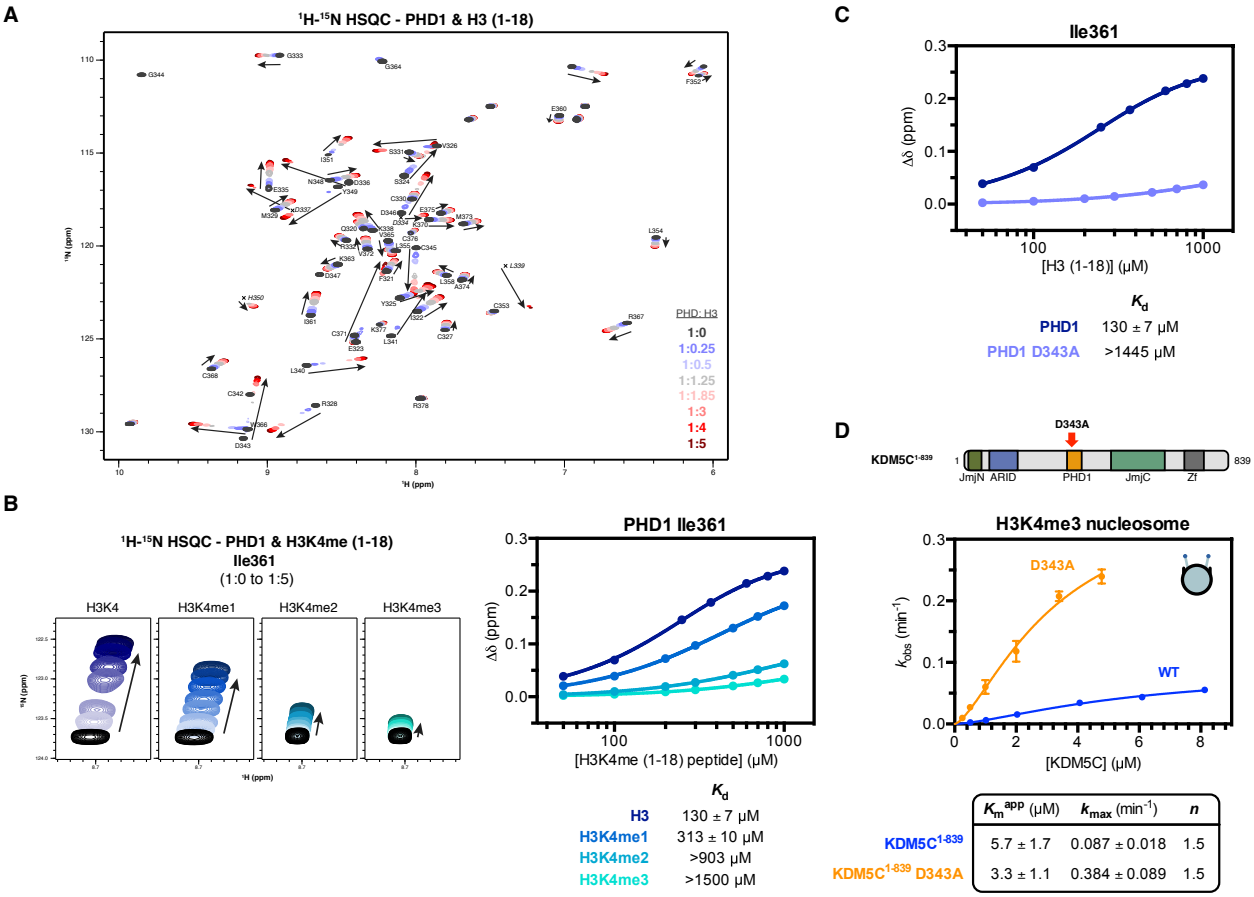

Figure 2. The PHD1 domain of KDM5C preferentially binds the unmodified H3 tail and has an inhibitory role towards demethylation on nucleosomes.
(A) 2D ^{1}H-^{15}N HSQC spectra of PHD1 titrated with increasing amounts of H3 (1-18) peptide with indicated molar ratios. Backbone assignments of residues in PHD1 are labeled. **(B)** 2D ^{1}H-^{15}N HSQC of I361 in PHD1 upon titration of H3K4me0/1/2/3 (1-18) peptides (*left*) with dissociation constants determined from the chemical shift change (Δδ) of I361 with standard error (*right*). Due to incomplete saturation of binding, a lower limit for the dissociation constant is presented for the H3K4me2/3 peptides. **(C)** Binding of the H3 (1-18) tail peptide by PHD1 and PHD1 D343A mutant measured by NMR titration HSQC experiments. The chemical shift change (Δδ) of I361 in PHD1 was fit to obtain dissociation constants with standard error. Due to incomplete saturation of binding by the D343A mutant, a lower limit for the dissociation constant is presented. **(D)** Demethylation kinetics of the H3K4me3 substrate nucleosome by wild type and PHD1 mutant KDM5C under single turnover conditions. Observed rates are fit to a cooperative kinetic model, with *n* denoting the Hill coefficient. Error bars represent SEM of at least two independent experiments ($n \geq 2$).

In order to investigate the function of PHD1 binding to the H3 tail in the context of the KDM5C enzyme, we sought to disrupt PHD1 binding through mutagenesis. We observe a dependence of binding on recognition of the H3R2 residue (Figure S2D). In addition, one of the largest chemical shift perturbations that occurs in PHD1 upon H3 tail binding is at the D343 residue, a homologous residue to D312 in KDM5A PHD1 that is part of the acidic pocket involved in H3R2 recognition (Figure S2E) (47). When mutated, it disrupts binding to H3 by KDM5A PHD1 (24). Similarly as in KDM5A, the D343A mutation decreases the affinity of KDM5C PHD1 to the H3 tail at least 10 fold (Figure 2C). This same mutation, when introduced into the $KDM5C^{1-839}$ enzyme, does not affect the catalytic rate of H3K4me3 peptide demethylation (Figure S2F). We then tested the effect of the D343A mutation on nucleosome binding and demethylation by KDM5C. While there is no significant change in nucleosome binding due to the D343A mutation in $KDM5C^{1-839}$ (Figure S2G), the PHD1 mutant enzyme demethylates the H3K4me3 nucleosome more rapidly than wild type $KDM5C^{1-839}$, with a ~4 fold increase of k_{max} (Figure 2D). This data supports an inhibitory role of the PHD1 domain during catalysis on nucleosomes by KDM5C. This inhibitory role is in stark contrast to that observed for the PHD1 domain in KDM5A, where binding of the H3 tail to PHD1 is stimulatory towards *in vitro* demethylation, suggesting a unique regulation of KDM5C.

KDM5C recognizes linker DNA in the absence of H3K4me3

In contrast to the inhibition of KDM5C demethylation by the PHD1 domain alone, the combined effect of the ARID and PHD1 domains appears to be catalytic enhancement on nucleosomes (Figure 1C). The ARID domains of KDM5A/B have been previously shown to recognize DNA, a feature likely conserved in KDM5C (13, 14). The minor contribution of the ARID and PHD1 domain region towards nucleosome binding (Figure 1B) suggests possible occlusion of ARID's DNA binding surface or an unfavorable orientation of the ARID domain towards DNA

engagement. To facilitate possible DNA engagement, we interrogated binding of KDM5C$^{1-839}$ towards nucleosomes containing 20 bp flanking DNA on both ends (187 bp nucleosome). Strikingly, we observe at least a 3-fold gain in affinity towards the 187 bp nucleosome (Figure 3A), demonstrating that KDM5C is capable of recognizing linker DNA. We next interrogated linker DNA recognition in the presence of the H3K4me3 substrate, as recognition of both could facilitate recruitment of KDM5C to its target sites in euchromatin (28). Intriguingly, KDM5C$^{1-839}$ has similar binding affinity for both the core and flanking DNA-containing H3K4me3 nucleosome, with K_d^{app} of ~8 μM, indicating no engagement of linker DNA in the presence of the H3K4me3 substrate (Figure 3B).

Since KDM5C recognizes linker DNA only in the context of the unmodified nucleosome, we considered the possibility that ARID's ability to engage linker DNA is coupled to binding of the H3 tail product, formed during demethylation, to the PHD1 domain. To test this model, we interrogated the effect of the PHD1 D343A mutation on the recognition of linker DNA by KDM5C. We find that PHD1 mutant KDM5C$^{1-839}$ D343A still retains the 3-fold affinity gain towards the unmodified 187 bp nucleosome (K_d^{app} = 3.6 μM) compared to the unmodified core nucleosome (K_d^{app} = 9.2 μM) (Figure 3C). In addition, unlike wild type KDM5C, the PHD1 mutant KDM5C displays a ~2 fold affinity gain towards the 187 bp H3K4me3 nucleosome (K_d^{app} = 5.3 μM), relative to the H3K4me3 core nucleosome (K_d^{app} = 9.3 μM) (Figure 3C). Although modest, this improved binding demonstrates that, unlike wild type, the PHD1 mutant KDM5C is capable of interacting with linker DNA in the presence of the H3K4me3 substrate.

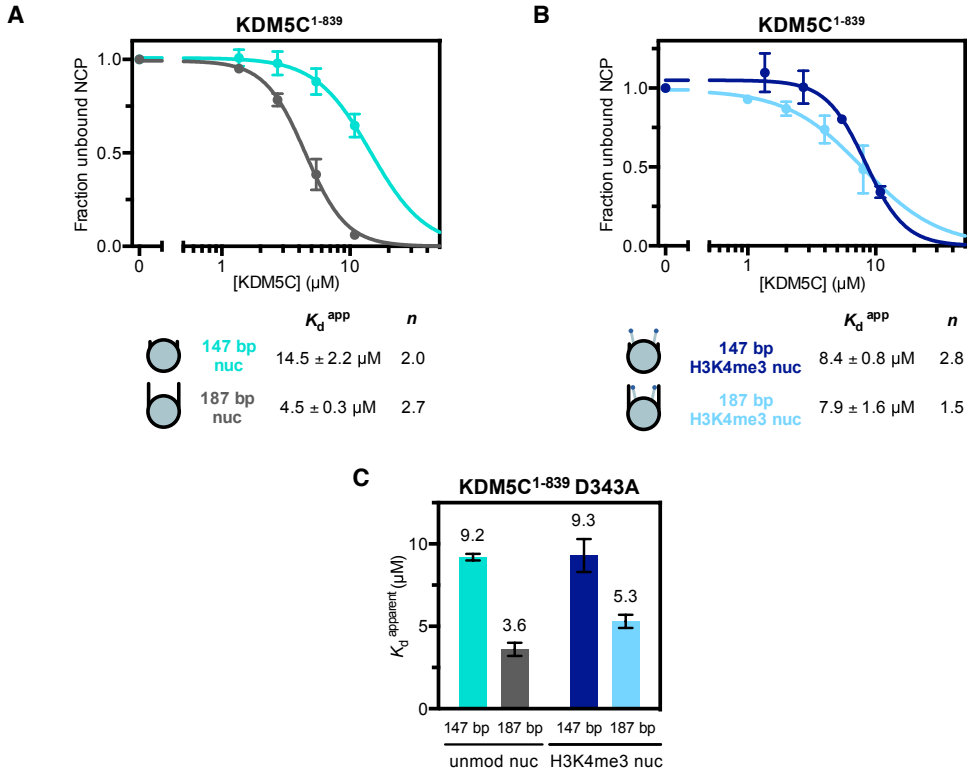

Figure 3. KDM5C recognizes linker DNA in the absence of H3K4me3 due to regulation by PHD1.
(A) Binding of KDM5C$^{1-839}$ to unmodified nucleosomes with and without 20 bp flanking DNA. Nucleosome binding curves were measured by EMSA and fit to a cooperative binding model to determine apparent dissociation constants (K_d^{app}), with n denoting the Hill coefficient (representative gel shift of KDM5C binding to the 187 bp nucleosome in Figure S3B). **(B)** Nucleosome binding curves of KDM5C$^{1-839}$ binding to substrate nucleosomes with and without 20 bp flanking DNA. **(C)** Nucleosome binding by PHD1 mutant KDM5C$^{1-839}$ D343A with apparent dissociation constants (K_d^{app}) measured by EMSA (binding curves in Figure S3C). All error bars represent SEM of at least two independent experiments ($n \geq 2$).

These findings suggest that linker DNA recognition by the ARID domain is regulated by the PHD1 domain. The ability of PHD1 mutant KDM5C to recognize linker DNA in the presence of H3K4me3 led us to hypothesize that, beyond disruption of H3 tail binding, the D343A PHD1 mutation might release any PHD1-imposed structural restrictions on the ARID domain, enabling recognition of DNA. This structural effect of the D343A PHD1 mutation may explain the catalytic enhancement caused by the PHD1 mutation on the substrate nucleosome (Figure 2D), as removal of restrictions on the ARID domain might enhance interactions with DNA that are beneficial during catalysis.

The recognition of linker DNA by KDM5C on unmodified but not substrate nucleosomes supports a model where binding of the H3 tail to PHD1 releases PHD1's structural restriction of the ARID domain, allowing it to bind linker DNA. However, the dual effects of the D343A PHD1 mutation and the affinity regime of the PHD1-H3 interaction prevents direct testing of the impact of the PHD1-H3 interaction on linker DNA recognition. To interrogate whether PHD1 could inhibit ARID's ability to bind DNA, we tested binding of free DNA to both wild type and PHD1 mutant $KDM5C^{1-839}$. The lack of an observable difference (Figure S3A) suggests that PHD1 does not directly inhibit ARID's DNA binding surface, but instead positions the ARID domain in an unfavorable orientation towards DNA engagement on the nucleosome.

Our findings of KDM5C nucleosome recognition and demethylation can be best explained by a regulatory model where PHD1 controls ARID-DNA recognition (Figure 4). Before catalysis, the H3K4me3 substrate is recognized and DNA binding is attenuated due to the restriction of ARID by PHD1 (state I). Basal demethylation is achieved through transient interactions of ARID with DNA during catalysis, which orients the catalytic domain towards the H3K4me3 tail. Release of the PHD1-imposed constraint on the ARID domain enables its improved interaction with DNA, leading to faster catalysis (state II). In our experiments, the D343A PHD1 mutation was used as a mechanistic probe to release the PHD1-imposed restriction on the ARID domain. In the context of chromatin, this release of the restriction on ARID could be achieved through binding of the H3 tail to PHD1, allowing for the regulation of demethylation by the surrounding chromatin environment. Formation of the H3 product, and its binding to PHD1, further reinforces interaction of KDM5C with chromatin by enabling linker DNA recognition by the ARID domain (state III).

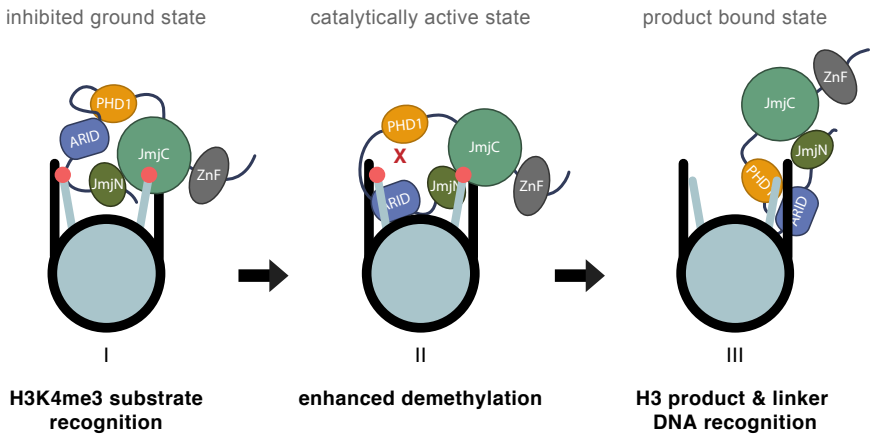

Figure 4. Model of KDM5C regulation by the ARID and PHD1 domains.
KDM5C recognizes H3K4me3 and binds to substrate nucleosomes through the catalytic domain (*pre-catalytic and inhibited ground state I)*. DNA binding in the presence of H3K4me3 is attenuated due to restriction of the ARID domain by PHD1. During demethylation, ARID and PHD1 make transient interactions with nucleosomes to orient the catalytic domain towards the H3K4me3 tail for productive demethylation. H3 tail binding to PHD1 releases the PHD1 interaction constraining the ARID domain, enabling ARID interaction with DNA to further enhance demethylation (*catalytically active state II).* After demethylation, binding of the product H3 tail to PHD1 further enables linker DNA binding by ARID (*post-catalytic and product bound state III).*

X-linked intellectual disability mutations alter nucleosome recognition and demethylation by KDM5C

Our proposed regulatory model provides a molecular framework for querying the effects of mutations in KDM5C that cause XLID (Figure 5A). Specifically, we sought to investigate the D87G and A388P mutations found at the beginning of ARID and immediately downstream of PHD1, respectively. The D87G mutation, associated with mild intellectual disability, has been demonstrated to have no effect on global H3K4me3 levels *in vivo* (41). The A388P mutation, associated with moderate intellectual disability, has also been shown to have no effect on global H3K4me3 levels *in vivo* but has been reported to reduce demethylase activity *in vitro* (2, 48). We initially interrogated nucleosome binding by KDM5C$^{1-839}$ D87G and A388P. Strikingly, relative to wild type KDM5C$^{1-839}$, we observe 4-9 fold enhanced binding of the XLID mutants to the unmodified core nucleosome (Figure 5B), suggesting that these mutations may be disrupting the occluded state of the ARID and PHD1 domain region, allowing them to engage in nucleosome

binding. We find that the ARID and PHD1 region is required for this enhanced nucleosome binding, as we observe no gain in nucleosome affinity due to the A388P mutation when the ARID and PHD1 region is removed (Figure S4A). Importantly, the gain in nucleosome affinity of the XLID mutants relative to wild type is more prominent on the unmodified core nucleosome than the substrate H3K4me3 core nucleosome, resulting in loss of specificity towards H3K4me3 by KDM5C due to the D87G and A388P mutations (Figure 5C).

As the XLID mutations cause an overall affinity gain towards both unmodified and substrate nucleosomes, we reasoned that the recognition of the shared common epitope of DNA, rather than the H3 tail, is altered in the mutants. Indeed, relative to wild type KDM5C$^{1-839}$, we observe a similar 4-5 fold gain in affinity by the XLID mutants towards the 187 bp nucleosome with flanking DNA, with both D87G and A388P mutants converging to a high nucleosome affinity of K_d^{app} ~1 μM (Figure 5D). As linker DNA recognition by KDM5C appears to be regulated by PHD1 (Figure 3C), we further interrogated linker DNA recognition by the D87G and A388P mutants. Both KDM5C$^{1-839}$ D87G and A388P are capable of recognizing linker DNA in the presence of H3K4me3, with a ~2 fold gain in affinity towards the 187 bp H3K4me3 nucleosome over the H3K4me3 core nucleosome (Figure 5E). These findings suggest that, similarly to the D343A PHD1 mutation (Figure 3C), the XLID mutations disrupt the PHD1-mediated restriction of the ARID domain towards linker DNA binding. Our findings are consistent with the model that these distinct XLID mutations are altering the conformational state of the ARID and PHD1 region, such that the ARID domain is in a more favorable orientation towards DNA binding on the nucleosome.

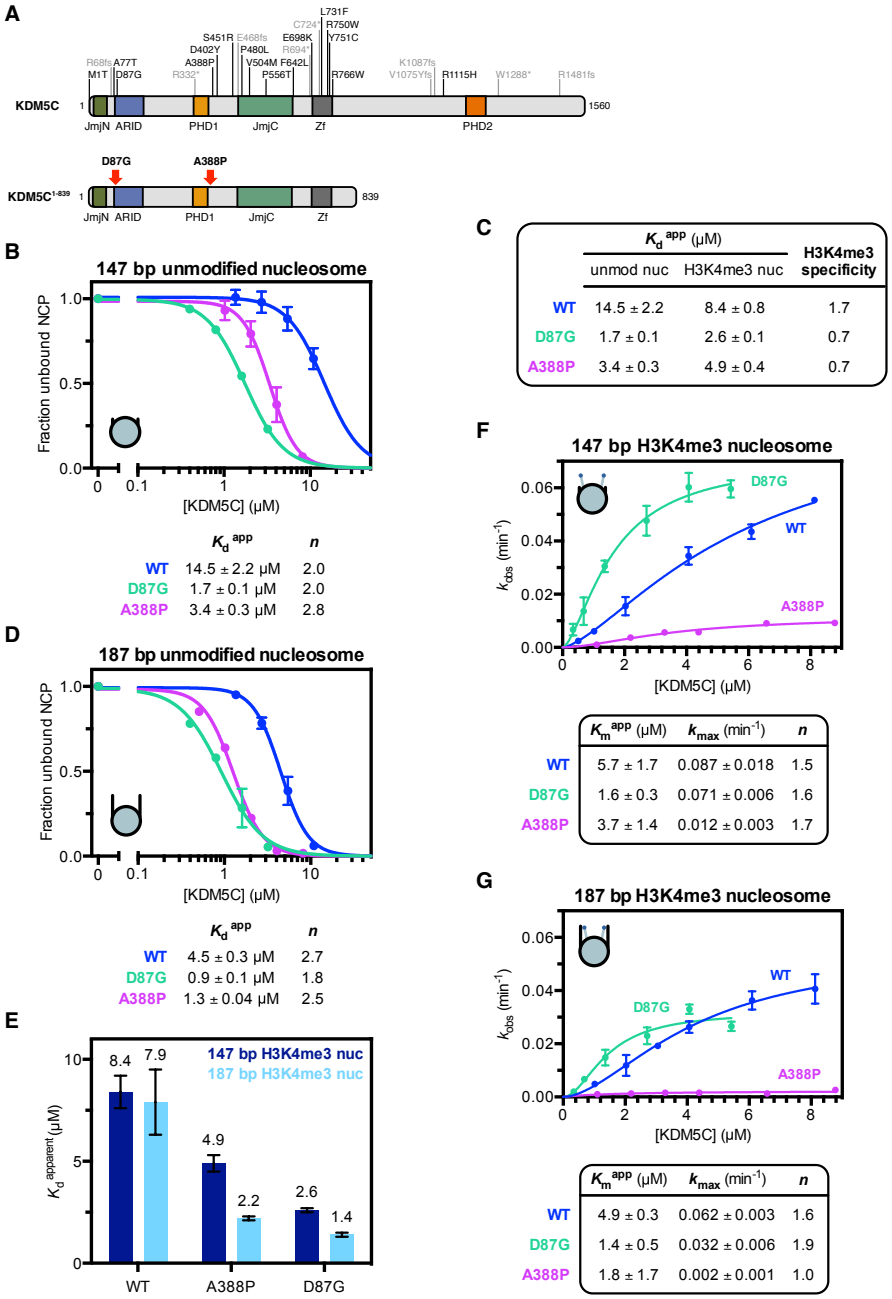

Figure 5. X-linked intellectual disability mutations enhance nucleosome binding by KDM5C and reduce demethylase activity in the presence of linker DNA.
(A) XLID mutations found in KDM5C (*top*) and the XLID mutations investigated in this study (*bottom*). **(B)** Unmodified core nucleosome binding by KDM5C$^{1-839}$ wild type, D87G, and A388P. Nucleosome binding curves were measured by EMSA and fit to a cooperative binding model to determine apparent dissociation constants (K_d^{app}), with *n* denoting the Hill coefficient. **(C)** Apparent dissociation constants (K_d^{app}) of binding by KDM5C$^{1-839}$ wild type, D87G, and A388P to unmodified and substrate core nucleosomes and resulting H3K4me3 fold specificity. **(D)** Binding curves of KDM5C$^{1-839}$ wild type, D87G, and A388P binding to the unmodified 187 bp nucleosome with 20 bp flanking DNA. **(E)** Binding of KDM5C$^{1-839}$ wild type, D87G, and A388P to substrate nucleosomes with and without 20 bp flanking DNA with apparent dissociation constants (K_d^{app}) measured by EMSA (binding curves in Figure S4C). **(F)** Demethylation kinetics of the core substrate nucleosome by KDM5C$^{1-839}$ wild type, D87G, and A388P under single turnover conditions. Observed rates are fit to a cooperative kinetic model, with *n* denoting the Hill coefficient. **(G)** Demethylation kinetics of the 187 bp substrate nucleosome by KDM5C$^{1-839}$ wild type, D87G, and A388P under single turnover conditions. All error bars represent SEM of at least two independent experiments ($n \geq 2$).

We next measured the demethylase activity of KDM5C$^{1-839}$ D87G and A388P towards the H3K4me3 core nucleosome substrate. Despite the XLID mutants sharing similar enhanced nucleosome binding, their effects on nucleosome demethylation differ. The A388P mutation impairs catalysis (k_{max}) by KDM5C by ~7 fold, while the D87G mutation increases catalytic efficiency (k_{max}/K_m^{app}) ~3 fold through an enhanced K_m^{app}, indicating both nonproductive and productive KDM5C conformations caused by these XLID mutations (Figure 5F). The reduced demethylase activity caused by the A388P mutation is consistent with previous findings of reduced *in vitro* demethylation, with the 7 fold reduction we observe on nucleosomes exceeding the previously reported 2 fold reduction on substrate peptide (2). The reduced demethylase activity due to the A388P mutation might be caused by distal structural impairment of the composite catalytic domain, as we observe reduced demethylase activity due to the A388P mutation in KDM5C$^{1-839}$ ΔAP (Figure S4B). In contrast, the D87G mutation does not appear to affect the catalytic domain, and instead the improved catalytic efficiency reflects the enhancement in nucleosome binding.

Unlike wild type KDM5C, these XLID mutants recognize linker DNA in the presence of H3K4me3. We then measured demethylase activity on the 187 bp H3K4me3 nucleosome. Demethylation by wild type KDM5C$^{1-839}$ is only minimally reduced on the flanking DNA-containing substrate nucleosome compared to the core substrate nucleosome (k_{max} ~ 0.06 min^{-1} vs k_{max} ~ 0.09 min^{-1}, respectively) (Figure 5F and 5G). Interestingly, we find that addition of linker DNA to the substrate nucleosome results in strong inhibition of catalysis by KDM5C$^{1-839}$ A388P, with a 6 fold reduction in k_{max} relative to the core substrate nucleosome (Figure 5G). Addition of linker DNA also reduces catalysis by KDM5C$^{1-839}$ D87G, although by a smaller amount of ~2 fold (Figure 5G). Despite maximal catalysis (k_{max}) by KDM5C$^{1-839}$ D87G being lower than wild type in the presence of linker DNA, the D87G mutant is still ~2 fold more efficient (k_{max}/K_m^{app}) due to its enhanced nucleosome binding. Regardless, enhanced linker DNA recognition caused by the XLID mutations

correlates with a reduction in the catalytic rate of H3K4me3 demethylation for nucleosomes with linker DNA. These findings may be particularly relevant to the dysregulation of KDM5C demethylation at euchromatic loci, where this enzyme predominantly functions (28, 31).

DISCUSSION

Different reader and regulatory domains within chromatin binding proteins and modifying enzymes influence their activity and substrate specificity by recognizing distinct chromatin states through distinguishing features on the nucleosome, histone modifications, and surrounding DNA. Emerging structural studies of chromatin modifying enzymes in complex with nucleosomes have highlighted these multivalent interactions, with increasing observations of interactions with DNA contributing to nucleosome engagement by histone modifying enzymes (49–58). Despite the unique insertion of the ARID and PHD1 reader domains in the composite catalytic domain, the function of accessory domains within the KDM5 demethylase family has not been explored on nucleosomes. Here, we provide critical insights into the hierarchy of regulation by these domains by investigating nucleosome recognition and catalysis in KDM5C, a unique member of the KDM5 family involved in regulation of neuronal gene transcription. We find that ARID recognition of DNA, an interaction beneficial for KDM5C demethylation on the nucleosome, is regulated by the PHD1 domain, allowing for sensing and specificity towards the H3K4me3 substrate. These interdomain interactions are disrupted by the D87G and A388P XLID mutations adjacent to the ARID and PHD1 domains, resulting in enhanced DNA binding and loss of H3K4me3 specificity due to an altered conformational state of KDM5C. This altered conformational state is nonproductive towards demethylation at target euchromatin sites of KDM5C, as enhanced DNA recognition by XLID mutants causes reduced demethylase activity in the presence of linker DNA.

Our finding of the overall beneficial role of the ARID and PHD1 region towards catalysis on nucleosomes can be rationalized by favorable transient interactions of the ARID domain with DNA to better position the catalytic domains towards the H3K4me3 tail substrate. This is supported by the previous observation that the ARID domain of KDM5C is required for its demethylase activity *in vivo* but not for its chromatin association (11). This role of the ARID domain in productive nucleosome demethylation may be conserved within the KDM5 family, as the ARID domain has also been found to be required for *in vivo* demethylation by KDM5B and the Drosophila KDM5 homolog Lid (4, 10, 12). The ARID domain may be required for nucleosome demethylation in order to displace the H3K4me3 tail from interacting with DNA, making it accessible for engagement by the catalytic domain. This histone tail displacement function has been proposed for DNA binding reader domain modules and for the LSD1/CoREST complex, where the SANT2 domain interacts with nucleosomal DNA to displace the H3 tail for engagement by the LSD1 active site (46, 57, 59, 60).

In contrast to the likely beneficial role of the ARID domain, we observe an unexpected inhibitory role of PHD1 towards KDM5C demethylation. This finding suggests differential regulation by PHD1 in the KDM5 family, as PHD1 binding has a stimulatory role towards *in vitro* demethylation in KDM5A/B, and PHD1 has been previously shown to be required for demethylase activity *in vivo* for KDM5B and Lid (4, 10, 24, 25, 27). Our data suggests this inhibitory role is achieved through PHD1-mediated restriction of the ARID domain's ability to engage DNA on the nucleosome. With weak affinity, a binding-induced conformational change, and indifference for a free N-terminus (Figure S5), ligand recognition by PHD1 in KDM5C is strikingly different from that observed for the PHD1 domains in KDM5A and KDM5B. While further work is needed to identify how PHD1 interacts within KDM5C to influence the ARID domain, the unique linker region between ARID and PHD1 of KDM5C, which varies in sequence and is longer compared to other KDM5 members (Figure S6), may contribute to distinct regulation by PHD1. Although we are

unable to directly test the effect of H3 tail binding to PHD1 on DNA recognition, we hypothesize that the resulting conformational change might release the restriction of the ARID domain, allowing for the tuning of KDM5C activity in different chromatin environments. As a consequence, H3 tail binding by PHD1 might be stimulatory towards demethylation, as observed upon binding by PHD1 in KDM5A/B, through a mechanistically distinct relief of negative regulation in KDM5C (Figure 4).

Unexpectedly, KDM5C recognizes linker DNA in the presence of the unmodified H3 tail but not in the presence of the H3K4me3 substrate, with this discrimination seemingly established through regulatory coupling of ARID to PHD1. While the function of this linker DNA recognition is unclear, it may serve to retain KDM5C at its target promoter and enhancer sites within open chromatin after demethylation. It may also enable processive demethylation of adjacent nucleosomes in euchromatin by KDM5C. Interestingly, the recognition of linker DNA has been observed in the mechanistically unrelated H3K4me1/2 histone demethylase LSD1/KDM1A, where demethylase activity is in contrast stimulated by linker DNA (49, 61). The H3K36me1/2 demethylase KDM2A is also capable of recognizing linker DNA, where it is specifically recruited to unmethylated CpG islands at gene promoters through its ZF-CxxC domain (62, 63). These findings suggest that recognition of the chromatin state with accessible linker DNA may be utilized by histone modifying enzymes that function on euchromatin. While the specificity of DNA recognition by the ARID domain remains to be fully characterized, it is evident that the sensing of the H3K4me3 substrate tail by KDM5C is hierarchical over recognition of linker DNA, a feature accessible in open chromatin. This sensing of H3K4me3 could be facilitated by an accessible KDM5C active site allowing catalytic domain interactions with the substrate H3K4me3 tail. This observed hierarchy, coupled with KDM5C's overall weak affinity towards nucleosomes and dampened demethylase activity due to regulation by PHD1, suggests tunable demethylation by

KDM5C. We thus propose a H3K4me3 surveillance model of KDM5C-catalyzed demethylation on chromatin (Figure 6), which is well suited for its physiological role in fine tuning gene expression through H3K4me3 demethylation at enhancers and promoters of genes, as well as its role in genome surveillance by preventing activation of non-neuronal genes in adult neurons (28, 31).

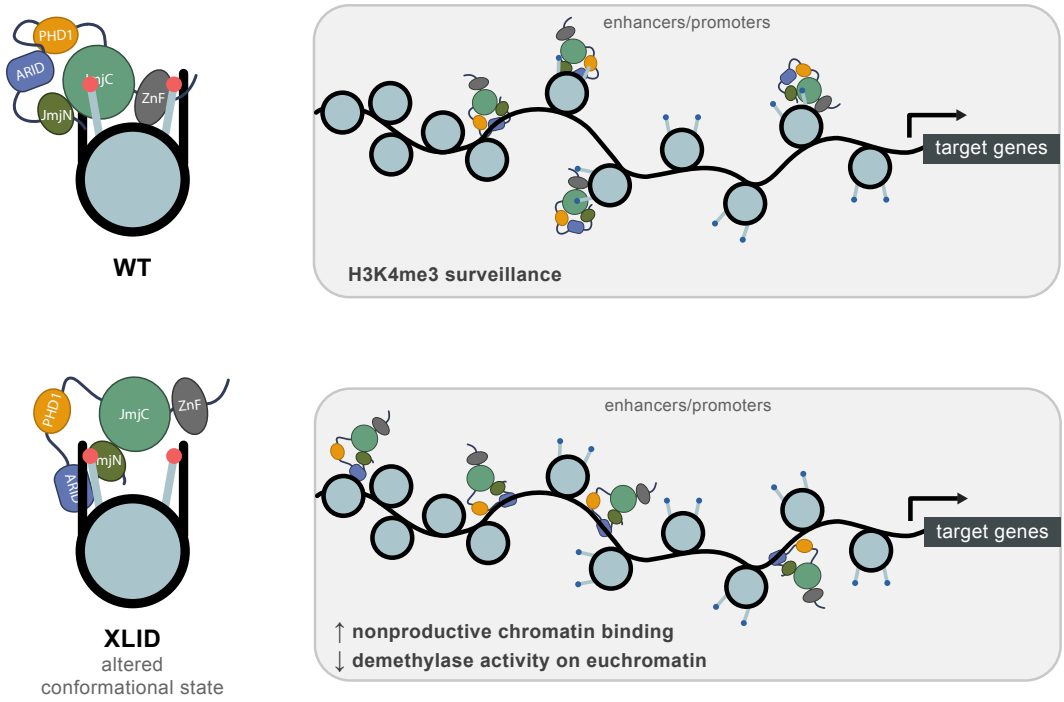

Figure 6. Model of H3K4me3 surveillance by KDM5C and dysregulation by XLID mutations on chromatin. Proposed function of H3K4me3 surveillance and demethylation by KDM5C on its target chromatin regions at gene promoters and enhancers (*top*). Proposed altered conformational state of the ARID and PHD1 region in KDM5C due to XLID mutations in this region disrupting hypothesized interdomain interactions, and predicted consequences on chromatin recognition and demethylation at KDM5C target sites (*bottom*).

Our findings show that the regulation of DNA recognition by KDM5C is disrupted by the D87G and A388P XLID mutations adjacent to the ARID and PHD1 domains, such that nucleosome binding is significantly enhanced, H3K4me3 specificity is lost, and demethylase activity is sensitized to inhibition by linker DNA. The location of these mutations support our model of restriction of the ARID domain by PHD1 towards DNA engagement on the nucleosome, where the XLID mutations disrupt these domain interactions and alter the conformational state of the

ARID and PHD1 region. Beyond disruption of histone demethylase activity, our findings suggest an additional mechanism of dysregulation of KDM5C in XLID, that of nonproductive enhanced chromatin engagement and differential dysregulation of demethylation at different loci depending on the chromatin state of accessible linker DNA (Figure 6). The A388P mutation appears to distally disrupt the catalytic domain in addition to affecting the conformational state of the ARID and PHD1 region, causing significantly reduced activity on nucleosomes that exceed previous reports using peptide substrates (2). Despite these *in vitro* observations, global H3K4me3 levels have been found to be unaffected with human KDM5C A388P *in vivo*, in contrast to increased global H3K4me3 levels observed in a Drosophila intellectual disability model with A512P mutant KDM5 Lid, signifying that further work is needed to profile H3K4me3 levels at genomic target regions affected by XLID mutations in human KDM5C (48, 64). Furthermore, our findings show that the demethylase activity of KDM5C D87G varies relative to wild type as a function of the presence of linker DNA, which might account for the unaffected global H3K4me3 levels previously observed with this D87G mutation (41). Interestingly, a gain of gene repressive function has been observed for the Y751C XLID mutation, where higher protein levels and lower H3K4me3 levels were found at the promoter of a down regulated gene unique to the Y751C mutant (65). This further illustrates locus specific consequences and possible enhanced chromatin binding, despite the reported lower *in vitro* peptide demethylation and unaffected global H3K4me3 levels by this mutant (2, 65). Enhanced chromatin association has been recently reported as a mechanism of cancer mutations occuring in the acyl histone-binding YEATS reader domain of ENL, conferring a gain of function in recruitment towards active transcription (66).

Our findings suggest that the chromatin environment, in particular the presence of accessible linker DNA, could govern altered demethylation and nonproductive chromatin recognition by KDM5C in XLID. Euchromatin-specific dysregulation of KDM5C demethylation might account for the hard-to-reconcile discrepancies between reported *in vitro* demethylase

activities of KDM5C XLID mutants and their effect on H3K4me3 levels. While additional XLID mutations elsewhere in KDM5C remain to be tested, it is possible that these dispersed mutations share a common mechanism of disrupted communication between domains that regulate the sensing of chromatin and demethylation by KDM5C.

EXPERIMENTAL PROCEDURES

Generation of KDM5C constructs

Human KDM5C gene was obtained from Harvard PlasmID (HsCD00337804) and Q175 was inserted to obtain the canonical isoform (NP_004178.2). KDM5C residues 1 to 839 were cloned into a pET28b SUMO-tag vector to produce 6xHis-SUMO-KDM5C and was mutated by site-directed mutagenesis for point mutants. The $KDM5C^{1-839}$ ΔAP construct was cloned by replacing residues 83-378 with a 4xGly linker.

Purification of KDM5C constructs

Recombinant His-tagged SUMO-KDM5C constructs were expressed in BL21(DE3) *E. coli* in LB media containing 50 μM $ZnCl_2$ and 100 μM $FeCl_3$ through induction at OD_{600} ~0.6 using 100 μM IPTG followed by expression at 18 ºC overnight. Collected cells were resuspended in 50 mM HEPES pH 8, 500 mM KCl, 1 mM BME, 5 mM imidazole, and 1 mM PMSF, supplemented with EDTA-free Pierce protease inhibitor tablets (Thermo Fisher Scientific) and benzonase, and lysed by microfluidizer. Lysate was clarified with ultracentrifugation and the recovered supernatant was then purified by TALON metal affinity resin (total contact time under 2 hrs) at 4 ºC. The His-SUMO tag was then cleaved by SenP1 during overnight dialysis at 4 ºC in 50 mM HEPES pH 7.5, 150 mM KCl, and 5 mM BME. KDM5C constructs were then purified by anion exchange (MonoQ, GE Healthcare) and subsequent size exclusion (Superdex 200, GE Healthcare) chromatography in 50 mM HEPES pH 7.5 and 150 mM KCl. Fractions were concentrated and aliquots snap frozen in liquid nitrogen for storage at -80 ºC.

Nucleosomes

Recombinant human 5' biotinylated unmodified 147 bp mononucleosomes (16-0006), unmodified 187 bp mononucleosomes (16-2104), 5' biotinylated H3K4me3 147 bp mononucleosomes (16-

0316), and 5' biotinylated H3K4me3 187 bp mononucleosomes (16-2316) were purchased from Epicypher, Inc., in addition to biotinylated 601 sequence DNA (18-005). 187 bp nucleosomes contain the 20 bp sequences 5' GGACCCTATACGCGGCCGCC and GCCGGTCGCGAACAGCGACC 3' flanking the 601 positioning sequence. For use in binding and kinetic assays, stock nucleosomes were buffer exchanged into corresponding assay buffer using a Zeba micro spin desalting column (Thermo Scientific).

Nucleosome binding assays

Nucleosome and DNA binding was assessed by EMSA. 100 nM nucleosomes (0.5 pmol) and various concentrations of KDM5C were incubated in binding buffer (50 mM HEPES pH 7.5, 50 mM KCl, 1mM BME, 0.01% Tween-20, 0.01% BSA, 5% sucrose) for 1 hr on ice prior to analysis by native 7.5% PAGE. Samples were separated using pre-run gels by electrophoresis in 1xTris-Glycine buffer at 100V for 2 hrs at 4 ºC, stained using SYBR Gold for DNA visualization, and imaged using the ChemiDoc imaging system (Bio-Rad Laboratories). Bands were quantified using Bio-Rad Image Lab software to determine the fraction of unbound nucleosome to calculate apparent dissociation constants by fitting to the cooperative binding equation $Y=(X^n)/(K_d^n + X^n)$, where X is the concentration of KDM5C, n is the Hill coefficient, and K_d is the concentration of KDM5C at which nucleosomes are half bound.

Single turnover nucleosome demethylation kinetics

The demethylation of biotinylated H3K4me3 nucleosome was monitored under single turnover conditions (>10 fold excess of KDM5C over substrate) through the detection of H3K4me1/2 product nucleosome formation over time by TR-FRET of an anti-H3K4me1/2 donor with an anti-biotin acceptor reagent. Various concentrations of KDM5C were reacted with 25 nM 5' biotinylated H3K4me3 nucleosome in 50 mM HEPES pH 7.5, 50 mM KCl, 0.01% Tween-20, 0.01% BSA, 50 μM alpha-ketoglutarate, 50 μM ammonium iron(II) sulfate, and 500 μM ascorbic acid at room

temperature. 5 µL time points were taken and quenched with 1.33 mM EDTA then brought to 20 µL final volume for detection using 1 nM LANCE Ultra Europium anti-H3K4me1/2 antibody (TRF0402, PerkinElmer) and 50 nM LANCE Ultra Ulight-Streptavidin (TRF0102, PerkinElmer) in 0.5X LANCE detection buffer. Detection reagents were incubated with reaction time points for 2 hours at room temperature in 384 well white microplates (PerkinElmer OptiPlate-384) then TR-FRET emission at 665 nm and 615 nm by 320 nm excitation with 50 µs delay and 100 µs integration time was measured using a Molecular Devices SpectraMax M5e plate reader. TR-FRET was calculated as the 665/615 nm emission ratio and kinetic curves were fit to a single exponential function to determine k_{obs} of demethylation. k_{obs} parameters were then plotted as a function of KDM5C concentration and fit to the sigmoidal kinetic equation $Y=k_{max}*X^n/(K_{half}^n + X^n)$ using GraphPad Prism to determine k_{max} and K_m^{app} parameters of demethylation.

Purification of PHD1 for NMR

PHD1 (KDM5C residues 318-378) was cloned into a pET28b SUMO-tag vector to express recombinant 6xHis-SUMO-PHD1 in BL21(DE3) *E. coli* in metal supplemented M9 minimal medium containing $^{15}NH_4Cl$ (Cambridge Isotope Laboratories). ^{13}C-glucose (Cambridge Isotope Laboratories) was used in medium for expression of ^{15}N, ^{13}C-labeled PHD1. Expression was induced at OD_{600} ~0.6 using 1 mM IPTG for expression at 18 ºC overnight. Collected cells were resuspended in 50 mM HEPES pH 8, 500 mM KCl, 5 mM BME, 10 mM imidazole, and 1 mM PMSF, supplemented with benzonase, and lysed by sonication. Lysate was clarified with ultracentrifugation and the recovered supernatant was then purified by Ni-NTA affinity resin. The His-SUMO tag was then cleaved by SenP1 during overnight dialysis at 4 ºC in 50 mM HEPES pH 7.5, 150 mM KCl, 50 µM $ZnCl_2$ and 10 mM BME. Cleaved His-SUMO tag and SenP1 was captured by passing through Ni-NTA affinity resin and flow-through was then purified by anion exchange (MonoQ) chromatography in starting buffer of 50 mM HEPES pH 7.5, 150 mM KCl, 50 µM $ZnCl_2$

and 10 mM BME. Flow-through MonoQ fractions containing PHD1 were concentrated and aliquots snap frozen in liquid nitrogen for storage at -80 ºC.

PHD1 NMR and histone peptide NMR titrations

For backbone assignment of KDM5C PHD1, 400 μM ^{15}N, ^{13}C-labeled PHD1 in 50 mM HEPES pH 7.5, 50 mM KCl, 5 mM BME, 50 μM $ZnCl_2$, and 5% D_2O was used to perform 3D triple-resonance CBCA(CO)NH and CBCANH experiments at 298K using a 500 MHz Bruker spectrometer equipped with a cryoprobe. Triple-resonance experiments were also performed using 400 μM ^{15}N, ^{13}C-labeled PHD1 bound to 2 mM H3 (1-18) peptide (1:5 ratio) to assign broadened backbone residues in apo spectra. 3D spectra were processed using NMRPipe then analyzed and assigned using CcpNMR Analysis. Out of 56 assignable residues, 54 in apo PHD1 and 53 residues in H3 bound PHD1 were assigned.

For 2D ^{1}H-^{15}N HSQC spectra of KDM5C PHD1, 200 μM ^{15}N-labeled PHD1 in 50 mM HEPES pH 7.5, 50 mM KCl, 5 mM BME, 50 μM $ZnCl_2$, and 5% D_2O was used to obtain 2D spectra at 298K using a 800 MHz Bruker spectrometer equipped with a cryoprobe. Chemical-shift perturbation experiments were performed by obtaining HSQC spectra with increasing concentrations of histone tail peptides (GenScript) up to 1:5 molar ratio of PHD1:peptide. Data were processed using Bruker TopSpin and analyzed using CcpNMR Analysis. Chemical shifts were scaled and calculated as $\Delta\delta = \mathrm{sqrt}(((\Delta\delta H)^2+(\Delta\delta N/5)^2) / 2)$. Chemical shift values were then plotted as a function of histone peptide concentration and fit to the quadratic binding equation $Y=((X+P_T+K_d)-\mathrm{sqrt}((X+P_T+K_d)^2-4*P_T*X))*(Y_{max}-Y_{min})/(2*P_T)$, where X is the concentration of peptide and P_T is the concentration of PHD1, using GraphPad Prism to determine K_d values.

Single turnover peptide demethylation kinetics

The demethylation of biotinylated H3K4me3 peptide was monitored under single turnover conditions (>10 fold excess of KDM5C over substrate) through the detection of H3K4me3 substrate loss over time by TR-FRET of an anti-rabbit IgG donor, recognizing an anti-H3K4me3 rabbit antibody, with an anti-biotin acceptor reagent. Various concentrations of KDM5C were reacted with 25 nM H3K4me3 (1-21)-biotin peptide (AS-64357, AnaSpec) in 50 mM HEPES pH 7.5, 50 mM KCl, 0.01% Tween-20, 0.01% BSA, 50 μM alpha-ketoglutarate, 50 μM ammonium iron(II) sulfate, and 500 μM ascorbic acid at room temperature. 2.5 μL time points were taken and quenched with 2 mM EDTA then brought to 20 μL final volume for detection using 1:500 dilution anti-H3K4me3 antibody (05-745R, EMD Millipore), 1 nM LANCE Ultra Europium anti-rabbit IgG antibody (PerkinElmer AD0082), and 50 nM LANCE Ultra Ulight-Streptavidin (PerkinElmer TRF0102) in 0.5X LANCE detection buffer. Detection reagents were added stepwise with 30 min incubation of anti-H3K4me3 antibody and Ulight-Streptavidin with reaction time points followed by 1 hr incubation with Europium anti-rabbit antibody in 384 well white microplates (PerkinElmer OptiPlate-384). TR-FRET emission at 665 nm and at 615 nm by 320 nm excitation with 50 μs delay and 100 μs integration time was measured using a Molecular Devices SpectraMax M5e plate reader. TR-FRET was calculated as the 665/615 nm emission ratio then subject to normalization to H3K4me3 substrate signal before demethylation. Kinetic curves were fit to a single exponential function, with the plateau set to nonspecific background of H3K4me2 product detection, to determine k_{obs} of the H3K4me3 demethylation step. k_{obs} parameters were then plotted as a function of KDM5C concentration and fit to the sigmoidal kinetic equation $Y=k_{max}*X^n/(K_{half}^n + X^n)$ using GraphPad Prism to determine k_{max} and K_m' parameters of demethylation.

Multiple turnover peptide demethylation kinetics

A fluorescence-based enzyme coupled assay was used to detect the formaldehyde product of demethylation of H3K4me3 peptide under multiple turnover conditions (excess of substrate peptide over KDM5C). Various concentrations of H3K4me3 (1-21) substrate peptide (GenScript) were added with 1mM alpha-ketoglutarate to initiate demethylation by ~1 μM KDM5C in 50 mM HEPES pH 7.5, 50 mM KCl, 50 μM ammonium iron(II) sulfate, 2 mM ascorbic acid, 2 mM NAD+, and 0.05 U formaldehyde dehydrogenase (Sigma-Aldrich) at room temperature. Upon initiation, fluorescence (350 nm excitation, 460 nm emission) was measured in 20 sec intervals over 30 min using a Molecular Devices SpectraMax M5e plate reader. NADH standards were used to convert fluorescence to the rate of product concentration formed. Initial rates of the first 3 min of demethylation were plotted as a function of substrate concentration and fit to the tight-binding quadratic velocity equation $Y=V_{max}*((X+E_T+K_m)-sqrt((X+E_T+K_m)^2-4*E_T*X))/(2*E_T)$ using GraphPad Prism to determine Michaelis-Menten kinetic parameters of demethylation.

Histone peptide binding kinetics

Bio-layer interferometry was used to measure binding kinetics of histone peptides to biotinylated Avitag-PHD1. Avitag followed by a linker was inserted into pET28b SUMO-PHD1$^{318-378}$ to generate recombinant endogenously biotinylated 6xHis-SUMO-Avitag-$(GS)_2$-PHD1 through coexpression with BirA in BL21(DE3) *E. coli* in 2xTY media containing 50 μM $ZnCl_2$ and 50 μM biotin. Expression was induced at OD_{600} ~0.7 using 0.4 mM IPTG for expression at 18 ºC overnight. Collected cells were resuspended in 50 mM HEPES pH 8, 500 mM KCl, 5 mM BME, 10 mM imidazole, 50 μM biotin, and 1 mM PMSF, supplemented with benzonase, and lysed by sonication. Lysate was clarified with ultracentrifugation and the recovered supernatant was then purified by Ni-NTA affinity resin. The His-SUMO tag was then cleaved by SenP1 during overnight dialysis at 4 ºC in 50 mM HEPES pH 8, 150 mM KCl, 50 μM $ZnCl_2$ and 10 mM BME. Cleaved His-SUMO tag and SenP1 was captured by passing through Ni-NTA affinity resin and flow-through

was then purified by anion exchange (MonoQ) chromatography in starting buffer of 50 mM HEPES pH 8, 150 mM KCl, 50 μM $ZnCl_2$ and 10 mM BME. Flow-through MonoQ fractions containing Avitag-PHD1 were analyzed by western blotting to identify biotinylated fractions, which were then concentrated and aliquots snap frozen in liquid nitrogen for storage at -80 ºC. Using the Octet Red384 system (ForteBio) at 1000 rpm and 25 ºC, 100 nM Avitag-PHD1 was loaded onto streptavidin biosensors (ForteBio) for 10 min in assay buffer (50 mM HEPES pH 8, 50 mM KCl, 50 μM $ZnCl_2$, 5 mM BME, and 0.05% Tween-20) followed by 120 sec baseline then association and dissociation of 100 μM peptide (GenScript) in assay buffer. Data were processed by subtracting a single reference experiment of loaded Avitag-PHD1 without peptide. A two phase exponential function was used to fit the biphasic kinetic data using Origin software.

ACKNOWLEDGMENTS

We thank Barbara Panning, Geeta Narlikar, John Gross, Daniele Canzio, Ryan Tibble, Cynthia Chio, and members of the Fujimori laboratory for helpful discussions and guidance. This work was supported by the UCSF Discovery Fellows program and National Science Foundation Graduate Research Fellowship to F. S. U. and by the National Institutes of Health (R01 GM114044, R01 GM114044-03S1, and R01 CA250459) to D. G. F.

REFERENCES

1. Kimura, H. (2013) Histone modifications for human epigenome analysis. *Journal of Human Genetics*. **58**, 439–445
2. Iwase, S., Lan, F., Bayliss, P., de la Torre-Ubieta, L., Huarte, M., Qi, H. H., Whetstine, J. R., Bonni, A., Roberts, T. M., and Shi, Y. (2007) The X-linked mental retardation gene SMCX/JARID1C defines a family of histone H3 lysine 4 demethylases. *Cell*. **128**, 1077–1088
3. Klose, R. J., Yan, Q., Tothova, Z., Yamane, K., Erdjument-Bromage, H., Tempst, P., Gilliland, D. G., Zhang, Y., and Kaelin, W. G., Jr (2007) The retinoblastoma binding protein RBP2 is an H3K4 demethylase. *Cell*. **128**, 889–900
4. Yamane, K., Tateishi, K., Klose, R. J., Fang, J., Fabrizio, L. A., Erdjument-Bromage, H., Taylor-Papadimitriou, J., Tempst, P., and Zhang, Y. (2007) PLU-1 is an H3K4 demethylase involved in transcriptional repression and breast cancer cell proliferation. *Mol. Cell*. **25**, 801–812
5. Lee, M. G., Norman, J., Shilatifard, A., and Shiekhattar, R. (2007) Physical and functional association of a trimethyl H3K4 demethylase and Ring6a/MBLR, a polycomb-like protein. *Cell*. **128**, 877–887
6. Shi, Y., Lan, F., Matson, C., Mulligan, P., Whetstine, J. R., Cole, P. A., Casero, R. A., and Shi, Y. (2004) Histone demethylation mediated by the nuclear amine oxidase homolog LSD1. *Cell*. **119**, 941–953
7. Christensen, J., Agger, K., Cloos, P. A. C., Pasini, D., Rose, S., Sennels, L., Rappsilber, J., Hansen, K. H., Salcini, A. E., and Helin, K. (2007) RBP2 belongs to a family of demethylases, specific for tri-and dimethylated lysine 4 on histone 3. *Cell*. **128**, 1063–1076
8. Horton, J. R., Engstrom, A., Zoeller, E. L., Liu, X., Shanks, J. R., Zhang, X., Johns, M. A., Vertino, P. M., Fu, H., and Cheng, X. (2016) Characterization of a Linked Jumonji Domain of the KDM5/JARID1 Family of Histone H3 Lysine 4 Demethylases. *J. Biol. Chem.* **291**, 2631–2646
9. Johansson, C., Velupillai, S., Tumber, A., Szykowska, A., Hookway, E. S., Nowak, R. P., Strain-Damerell, C., Gileadi, C., Philpott, M., Burgess-Brown, N., Wu, N., Kopec, J., Nuzzi, A., Steuber, H., Egner, U., Badock, V., Munro, S., LaThangue, N. B., Westaway, S., Brown, J., Athanasou, N., Prinjha, R., Brennan, P. E., and Oppermann, U. (2016) Structural analysis of human KDM5B guides histone demethylase inhibitor development. *Nat. Chem. Biol.* **12**, 539–545
10. Li, L., Greer, C., Eisenman, R. N., and Secombe, J. (2010) Essential functions of the histone demethylase lid. *PLoS Genet.* **6**, e1001221
11. Brookes, E., Laurent, B., Õunap, K., Carroll, R., Moeschler, J. B., Field, M., Schwartz, C. E., Gecz, J., and Shi, Y. (2015) Mutations in the intellectual disability gene KDM5C reduce protein stability and demethylase activity. *Hum. Mol. Genet.* **24**, 2861–2872
12. Xiang, Y., Zhu, Z., Han, G., Ye, X., Xu, B., Peng, Z., Ma, Y., Yu, Y., Lin, H., Chen, A. P., and Chen, C. D. (2007) JARID1B is a histone H3 lysine 4 demethylase up-regulated in prostate cancer. *Proc. Natl. Acad. Sci. U. S. A.* **104**, 19226–19231
13. Tu, S., Teng, Y.-C., Yuan, C., Wu, Y.-T., Chan, M.-Y., Cheng, A.-N., Lin, P.-H., Juan, L.-J., and Tsai, M.-D. (2008) The ARID domain of the H3K4 demethylase RBP2 binds to a DNA CCGCCC motif. *Nat. Struct. Mol. Biol.* **15**, 419–421
14. Scibetta, A. G., Santangelo, S., Coleman, J., Hall, D., Chaplin, T., Copier, J., Catchpole, S., Burchell, J., and Taylor-Papadimitriou, J. (2007) Functional analysis of the transcription repressor PLU-1/JARID1B. *Mol. Cell. Biol.* **27**, 7220–7235
15. Lan, F., Collins, R. E., De Cegli, R., Alpatov, R., Horton, J. R., Shi, X., Gozani, O., Cheng, X., and Shi, Y. (2007) Recognition of unmethylated histone H3 lysine 4 links BHC80 to

LSD1-mediated gene repression. *Nature*. **448**, 718–722
16. Klein, B. J., Wang, X., Cui, G., Yuan, C., Botuyan, M. V., Lin, K., Lu, Y., Wang, X., Zhao, Y., Bruns, C. J., Mer, G., Shi, X., and Kutateladze, T. G. (2016) PHF20 Readers Link Methylation of Histone H3K4 and p53 with H4K16 Acetylation. *Cell Rep.* **17**, 1158–1170
17. Shi, X., Hong, T., Walter, K. L., Ewalt, M., Michishita, E., Hung, T., Carney, D., Peña, P., Lan, F., Kaadige, M. R., Lacoste, N., Cayrou, C., Davrazou, F., Saha, A., Cairns, B. R., Ayer, D. E., Kutateladze, T. G., Shi, Y., Côté, J., Chua, K. F., and Gozani, O. (2006) ING2 PHD domain links histone H3 lysine 4 methylation to active gene repression. *Nature*. **442**, 96–99
18. Li, H., Ilin, S., Wang, W., Duncan, E. M., Wysocka, J., Allis, C. D., and Patel, D. J. (2006) Molecular basis for site-specific read-out of histone H3K4me3 by the BPTF PHD finger of NURF. *Nature*. **442**, 91–95
19. Peña, P. V., Davrazou, F., Shi, X., Walter, K. L., Verkhusha, V. V., Gozani, O., Zhao, R., and Kutateladze, T. G. (2006) Molecular mechanism of histone H3K4me3 recognition by plant homeodomain of ING2. *Nature*. **442**, 100–103
20. Wysocka, J., Swigut, T., Xiao, H., Milne, T. A., Kwon, S. Y., Landry, J., Kauer, M., Tackett, A. J., Chait, B. T., Badenhorst, P., Wu, C., and Allis, C. D. (2006) A PHD finger of NURF couples histone H3 lysine 4 trimethylation with chromatin remodelling. *Nature*. **442**, 86–90
21. Sanchez, R., and Zhou, M.-M. (2011) The PHD finger: a versatile epigenome reader. *Trends Biochem. Sci.* **36**, 364–372
22. Klein, B. J., Piao, L., Xi, Y., Rincon-Arano, H., Rothbart, S. B., Peng, D., Wen, H., Larson, C., Zhang, X., Zheng, X., Cortazar, M. A., Peña, P. V., Mangan, A., Bentley, D. L., Strahl, B. D., Groudine, M., Li, W., Shi, X., and Kutateladze, T. G. (2014) The histone-H3K4-specific demethylase KDM5B binds to its substrate and product through distinct PHD fingers. *Cell Rep.* **6**, 325–335
23. Zhang, Y., Yang, H., Guo, X., Rong, N., Song, Y., Xu, Y., Lan, W., Zhang, X., Liu, M., Xu, Y., and Cao, C. (2014) The PHD1 finger of KDM5B recognizes unmodified H3K4 during the demethylation of histone H3K4me2/3 by KDM5B. *Protein Cell*. **5**, 837–850
24. Torres, I. O., Kuchenbecker, K. M., Nnadi, C. I., Fletterick, R. J., Kelly, M. J. S., and Fujimori, D. G. (2015) Histone demethylase KDM5A is regulated by its reader domain through a positive-feedback mechanism. *Nat. Commun.* **6**, 6204
25. Zhao, S., Chuh, K. N., Zhang, B., Dul, B. E., Thompson, R. E., Farrelly, L. A., Liu, X., Xu, N., Xue, Y., Roeder, R. G., Maze, I., Muir, T. W., and Li, H. (2021) Histone H3Q5 serotonylation stabilizes H3K4 methylation and potentiates its readout. *Proc. Natl. Acad. Sci. U. S. A.* 10.1073/pnas.2016742118
26. Wang, G. G., Song, J., Wang, Z., Dormann, H. L., Casadio, F., Li, H., Luo, J.-L., Patel, D. J., and Allis, C. D. (2009) Haematopoietic malignancies caused by dysregulation of a chromatin-binding PHD finger. *Nature*. **459**, 847–851
27. Longbotham, J. E., Chio, C. M., Dharmarajan, V., Trnka, M. J., Torres, I. O., Goswami, D., Ruiz, K., Burlingame, A. L., Griffin, P. R., and Fujimori, D. G. (2019) Histone H3 binding to the PHD1 domain of histone demethylase KDM5A enables active site remodeling. *Nat. Commun.* **10**, 94
28. Iwase, S., Brookes, E., Agarwal, S., Badeaux, A. I., Ito, H., Vallianatos, C. N., Tomassy, G. S., Kasza, T., Lin, G., Thompson, A., Gu, L., Kwan, K. Y., Chen, C., Sartor, M. A., Egan, B., Xu, J., and Shi, Y. (2016) A Mouse Model of X-linked Intellectual Disability Associated with Impaired Removal of Histone Methylation. *Cell Rep.* **14**, 1000–1009
29. Jensen, L. R., Bartenschlager, H., Rujirabanjerd, S., Tzschach, A., Nümann, A., Janecke, A. R., Spörle, R., Stricker, S., Raynaud, M., Nelson, J., Hackett, A., Fryns, J.-P., Chelly, J., de Brouwer, A. P., Hamel, B., Gecz, J., Ropers, H.-H., and Kuss, A. W. (2010) A distinctive gene expression fingerprint in mentally retarded male patients reflects disease-causing defects in the histone demethylase KDM5C. *Pathogenetics*. **3**, 2

30. Jensen, L. R., Amende, M., Gurok, U., Moser, B., Gimmel, V., Tzschach, A., Janecke, A. R., Tariverdian, G., Chelly, J., Fryns, J.-P., Van Esch, H., Kleefstra, T., Hamel, B., Moraine, C., Gecz, J., Turner, G., Reinhardt, R., Kalscheuer, V. M., Ropers, H.-H., and Lenzner, S. (2005) Mutations in the JARID1C gene, which is involved in transcriptional regulation and chromatin remodeling, cause X-linked mental retardation. *Am. J. Hum. Genet.* **76**, 227–236
31. Scandaglia, M., Lopez-Atalaya, J. P., Medrano-Fernandez, A., Lopez-Cascales, M. T., Del Blanco, B., Lipinski, M., Benito, E., Olivares, R., Iwase, S., Shi, Y., and Barco, A. (2017) Loss of Kdm5c Causes Spurious Transcription and Prevents the Fine-Tuning of Activity-Regulated Enhancers in Neurons. *Cell Rep.* **21**, 47–59
32. Outchkourov, N. S., Muiño, J. M., Kaufmann, K., van Ijcken, W. F. J., Groot Koerkamp, M. J., van Leenen, D., de Graaf, P., Holstege, F. C. P., Grosveld, F. G., and Timmers, H. T. M. (2013) Balancing of histone H3K4 methylation states by the Kdm5c/SMCX histone demethylase modulates promoter and enhancer function. *Cell Rep.* **3**, 1071–1079
33. Shen, H., Xu, W., Guo, R., Rong, B., Gu, L., Wang, Z., He, C., Zheng, L., Hu, X., Hu, Z., Shao, Z.-M., Yang, P., Wu, F., Shi, Y. G., Shi, Y., and Lan, F. (2016) Suppression of Enhancer Overactivation by a RACK7-Histone Demethylase Complex. *Cell*. **165**, 331–342
34. Gonçalves, T. F., Gonçalves, A. P., Fintelman Rodrigues, N., dos Santos, J. M., Pimentel, M. M. G., and Santos-Rebouças, C. B. (2014) KDM5C mutational screening among males with intellectual disability suggestive of X-Linked inheritance and review of the literature. *Eur. J. Med. Genet.* **57**, 138–144
35. Tzschach, A., Lenzner, S., Moser, B., Reinhardt, R., Chelly, J., Fryns, J.-P., Kleefstra, T., Raynaud, M., Turner, G., Ropers, H.-H., Kuss, A., and Jensen, L. R. (2006) Novel JARID1C/SMCX mutations in patients with X-linked mental retardation. *Hum. Mutat.* **27**, 389
36. Santos, C., Rodriguez-Revenga, L., Madrigal, I., Badenas, C., Pineda, M., and Milà, M. (2006) A novel mutation in JARID1C gene associated with mental retardation. *Eur. J. Hum. Genet.* **14**, 583–586
37. Abidi, F. E., Holloway, L., Moore, C. A., Weaver, D. D., Simensen, R. J., Stevenson, R. E., Rogers, R. C., and Schwartz, C. E. (2008) Mutations in JARID1C are associated with X-linked mental retardation, short stature and hyperreflexia. *J. Med. Genet.* **45**, 787–793
38. Rujirabanjerd, S., Nelson, J., Tarpey, P. S., Hackett, A., Edkins, S., Lucy Raymond, F., Schwartz, C. E., Turner, G., Iwase, S., Shi, Y., Andrew Futreal, P., Stratton, M. R., and Gecz, J. (2010) Identification and characterization of two novel JARID1C mutations: suggestion of an emerging genotype–phenotype correlation. *European Journal of Human Genetics*. **18**, 330–335
39. Xu, J., Burgoyne, P. S., and Arnold, A. P. (2002) Sex differences in sex chromosome gene expression in mouse brain. *Human Molecular Genetics*. **11**, 1409–1419
40. Vallianatos, C. N., Farrehi, C., Friez, M. J., Burmeister, M., Keegan, C. E., and Iwase, S. (2018) Altered Gene-Regulatory Function of KDM5C by a Novel Mutation Associated With Autism and Intellectual Disability. *Front. Mol. Neurosci.* **11**, 104
41. Tahiliani, M., Mei, P., Fang, R., Leonor, T., Rutenberg, M., Shimizu, F., Li, J., Rao, A., and Shi, Y. (2007) The histone H3K4 demethylase SMCX links REST target genes to X-linked mental retardation. *Nature*. **447**, 601–605
42. Jones, B. N., Quang-Dang, D.-U., Oku, Y., and Gross, J. D. (2008) A kinetic assay to monitor RNA decapping under single- turnover conditions. *Methods Enzymol.* **448**, 23–40
43. Gatchalian, J., Wang, X., Ikebe, J., Cox, K. L., Tencer, A. H., Zhang, Y., Burge, N. L., Di, L., Gibson, M. D., Musselman, C. A., Poirier, M. G., Kono, H., Hayes, J. J., and Kutateladze, T. G. (2017) Accessibility of the histone H3 tail in the nucleosome for binding of paired readers. *Nat. Commun.* **8**, 1489
44. Morrison, E. A., Bowerman, S., Sylvers, K. L., Wereszczynski, J., and Musselman, C. A. (2018) The conformation of the histone H3 tail inhibits association of the BPTF PHD finger

with the nucleosome. *Elife*. 10.7554/eLife.31481
45. Stützer, A., Liokatis, S., Kiesel, A., Schwarzer, D., Sprangers, R., Söding, J., Selenko, P., and Fischle, W. (2016) Modulations of DNA Contacts by Linker Histones and Post-translational Modifications Determine the Mobility and Modifiability of Nucleosomal H3 Tails. *Mol. Cell*. **61**, 247–259
46. Peng, Y., Li, S., Onufriev, A., Landsman, D., and Panchenko, A. R. (2021) Binding of regulatory proteins to nucleosomes is modulated by dynamic histone tails. *Nat. Commun.* **12**, 5280
47. Longbotham, J. E., Kelly, M. J. S., and Fujimori, D. G. (2021) Recognition of Histone H3 Methylation States by the PHD1 Domain of Histone Demethylase KDM5A. *ACS Chem. Biol.* 10.1021/acschembio.0c00976
48. Poeta, L., Padula, A., Lioi, M. B., van Bokhoven, H., and Miano, M. G. (2021) Analysis of a Set of KDM5C Regulatory Genes Mutated in Neurodevelopmental Disorders Identifies Temporal Coexpression Brain Signatures. *Genes* . 10.3390/genes12071088
49. Kim, S.-A., Zhu, J., Yennawar, N., Eek, P., and Tan, S. (2020) Crystal Structure of the LSD1/CoREST Histone Demethylase Bound to Its Nucleosome Substrate. *Mol. Cell*. **78**, 903–914.e4
50. Kasinath, V., Beck, C., Sauer, P., Poepsel, S., Kosmatka, J., Faini, M., Toso, D., Aebersold, R., and Nogales, E. (2021) JARID2 and AEBP2 regulate PRC2 in the presence of H2AK119ub1 and other histone modifications. *Science*. 10.1126/science.abc3393
51. Finogenova, K., Bonnet, J., Poepsel, S., Schäfer, I. B., Finkl, K., Schmid, K., Litz, C., Strauss, M., Benda, C., and Müller, J. (2020) Structural basis for PRC2 decoding of active histone methylation marks H3K36me2/3. *Elife*. 10.7554/eLife.61964
52. Worden, E. J., Zhang, X., and Wolberger, C. (2020) Structural basis for COMPASS recognition of an H2B-ubiquitinated nucleosome. *Elife*. 10.7554/eLife.53199
53. Li, W., Tian, W., Yuan, G., Deng, P., Sengupta, D., Cheng, Z., Cao, Y., Ren, J., Qin, Y., Zhou, Y., Jia, Y., Gozani, O., Patel, D. J., and Wang, Z. (2021) Molecular basis of nucleosomal H3K36 methylation by NSD methyltransferases. *Nature*. **590**, 498–503
54. Bilokapic, S., Suskiewicz, M. J., Ahel, I., and Halic, M. (2020) Bridging of DNA breaks activates PARP2–HPF1 to modify chromatin. *Nature*. **585**, 609–613
55. Bilokapic, S., and Halic, M. (2019) Nucleosome and ubiquitin position Set2 to methylate H3K36. *Nat. Commun.* **10**, 3795
56. Hsu, P. L., Shi, H., Leonen, C., Kang, J., Chatterjee, C., and Zheng, N. (2019) Structural Basis of H2B Ubiquitination-Dependent H3K4 Methylation by COMPASS. *Mol. Cell*. **76**, 712–723.e4
57. Marabelli, C., Marrocco, B., Pilotto, S., Chittori, S., Picaud, S., Marchese, S., Ciossani, G., Forneris, F., Filippakopoulos, P., Schoehn, G., Rhodes, D., Subramaniam, S., and Mattevi, A. (2019) A Tail-Based Mechanism Drives Nucleosome Demethylation by the LSD2/NPAC Multimeric Complex. *Cell Rep.* **27**, 387–399.e7
58. Poepsel, S., Kasinath, V., and Nogales, E. (2018) Cryo-EM structures of PRC2 simultaneously engaged with two functionally distinct nucleosomes. *Nat. Struct. Mol. Biol.* **25**, 154–162
59. Weaver, T. M., Morrison, E. A., and Musselman, C. A. (2018) Reading More than Histones: The Prevalence of Nucleic Acid Binding among Reader Domains. *Molecules*. 10.3390/molecules23102614
60. Pilotto, S., Speranzini, V., Tortorici, M., Durand, D., Fish, A., Valente, S., Forneris, F., Mai, A., Sixma, T. K., Vachette, P., and Mattevi, A. (2015) Interplay among nucleosomal DNA, histone tails, and corepressor CoREST underlies LSD1-mediated H3 demethylation. *Proc. Natl. Acad. Sci. U. S. A.* **112**, 2752–2757
61. Kim, S.-A., Chatterjee, N., Jennings, M. J., Bartholomew, B., and Tan, S. (2015) Extranucleosomal DNA enhances the activity of the LSD1/CoREST histone demethylase

complex. *Nucleic Acids Res.* **43**, 4868–4880
62. Zhou, J. C., Blackledge, N. P., Farcas, A. M., and Klose, R. J. (2012) Recognition of CpG island chromatin by KDM2A requires direct and specific interaction with linker DNA. *Mol. Cell. Biol.* **32**, 479–489
63. Blackledge, N. P., Zhou, J. C., Tolstorukov, M. Y., Farcas, A. M., Park, P. J., and Klose, R. J. (2010) CpG islands recruit a histone H3 lysine 36 demethylase. *Mol. Cell*. **38**, 179–190
64. Zamurrad, S., Hatch, H. A. M., Drelon, C., Belalcazar, H. M., and Secombe, J. (2018) A Drosophila Model of Intellectual Disability Caused by Mutations in the Histone Demethylase KDM5. *Cell Rep.* **22**, 2359–2369
65. Wei, G., Deng, X., Agarwal, S., Iwase, S., Disteche, C., and Xu, J. (2016) Patient Mutations of the Intellectual Disability Gene KDM5C Downregulate Netrin G2 and Suppress Neurite Growth in Neuro2a Cells. *Journal of Molecular Neuroscience*. **60**, 33–45
66. Wan, L., Chong, S., Xuan, F., Liang, A., Cui, X., Gates, L., Carroll, T. S., Li, Y., Feng, L., Chen, G., Wang, S.-P., Ortiz, M. V., Daley, S. K., Wang, X., Xuan, H., Kentsis, A., Muir, T. W., Roeder, R. G., Li, H., Li, W., Tjian, R., Wen, H., and David Allis, C. (2020) Impaired cell fate through gain-of-function mutations in a chromatin reader. *Nature*. **577**, 121–126

SUPPORTING INFORMATION

A

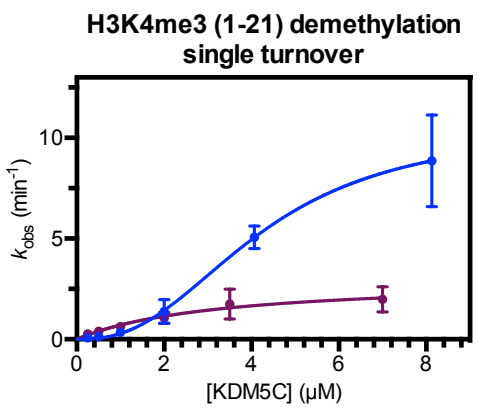

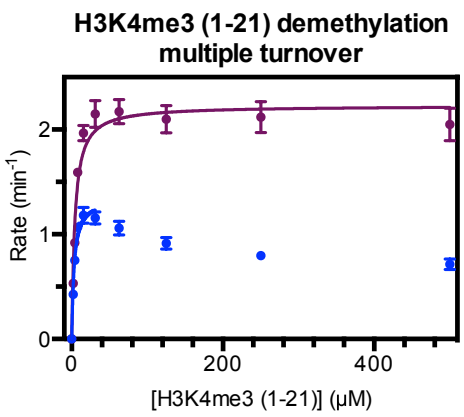

	K_m' (μM)	k_{max} (min^{-1})	n
KDM5C$^{1-839}$	4.2 ± 0.1	10.6 ± 0.3	2.5
KDM5C$^{1-839}$ ΔAP	3.3 ± 0.9	3.0 ± 0.4	1.0

	K_m (μM)	k_{cat} (min^{-1})
KDM5C$^{1-839}$	2.6 ± 0.7	1.34 ± 0.08
KDM5C$^{1-839}$ ΔAP	3.6 ± 0.7	2.22 ± 0.07

B

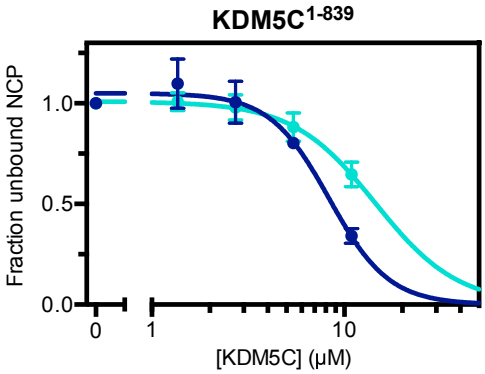

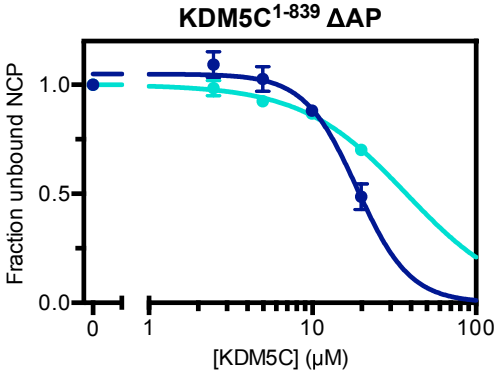

	K_d^{app}	n
H3K4me3 nuc	8.4 ± 0.8 μM	2.8
unmod nuc	14.5 ± 2.2 μM	2.0

	K_d^{app}	n
H3K4me3 nuc	18.7 ± 1.2 μM	2.7
unmod nuc	37.5 ± 5.0 μM	1.4

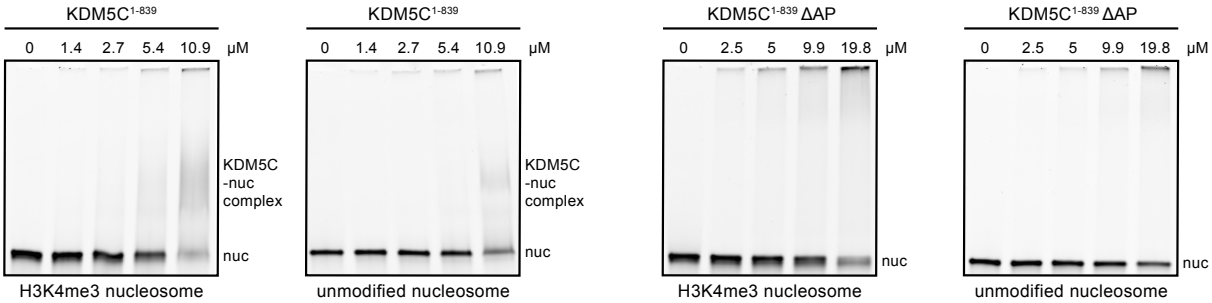

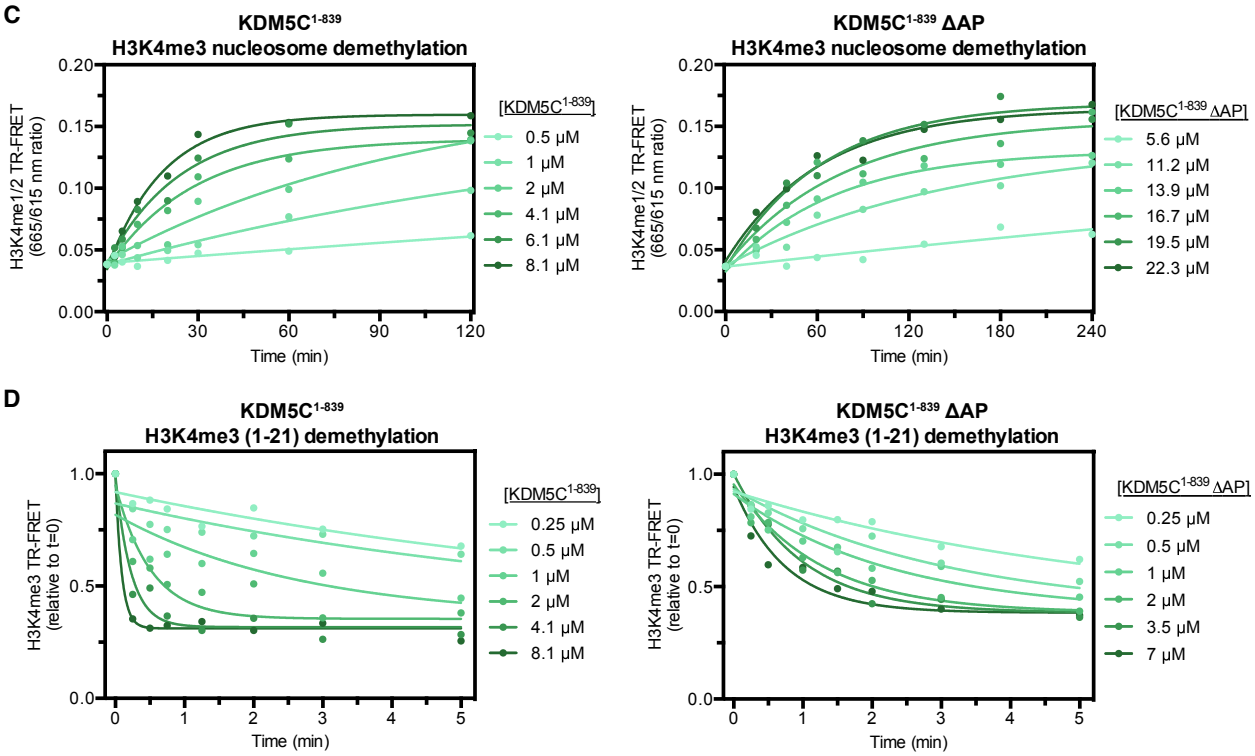

Figure S1. Related to Figure 1.
(A) H3K4me3 substrate peptide demethylation by KDM5C constructs. *Left*: Demethylation kinetics of the H3K4me3 (1-21) substrate peptide by KDM5C constructs under single turnover conditions measured by a TR-FRET based kinetic assay. Observed rates are fit to a cooperative kinetic model, with *n* denoting the Hill coefficient. Representative kinetic traces used to determine observed demethylation rates are in Figure S1D. *Right*: Demethylation kinetics of the H3K4me3 (1-21) substrate peptide by KDM5C constructs under multiple turnover conditions measured by a formaldehyde release based kinetic assay. Deletion of the ARID and PHD1 region results in higher demethylase activity on the substrate peptide under multiple turnover conditions due to loss of substrate inhibition caused by this region. **(B)** Unmodified and substrate core nucleosome binding by KDM5C$^{1-839}$ and KDM5C$^{1-839}$ ΔAP. Nucleosome binding curves were measured by EMSA and fit to a cooperative binding model to determine apparent dissociation constants (K_d^{app}), with *n* denoting the Hill coefficient (*top*). Representative gel shifts of KDM5C binding to nucleosomes (*bottom*). **(C)** Representative demethylation kinetic traces of substrate nucleosome demethylation by KDM5C constructs (*left*: KDM5C$^{1-839}$, *right*: KDM5C$^{1-839}$ ΔAP) under single turnover conditions using TR-FRET based kinetic assay detecting formation of the H3K4me1/2 product nucleosome over time. Observed rates (k_{obs}) are obtained by fitting kinetic traces to an exponential function. **(D)** Representative demethylation kinetic traces of substrate peptide demethylation by KDM5C constructs (*left*: KDM5C$^{1-839}$, *right*: KDM5C$^{1-839}$ ΔAP) under single turnover conditions using TR-FRET based kinetic assay detecting loss of the H3K4me3 substrate peptide over time. Observed rates (k_{obs}) are obtained by fitting kinetic traces to an exponential function. All error bars represent SEM of at least two independent experiments ($n \geq 2$).

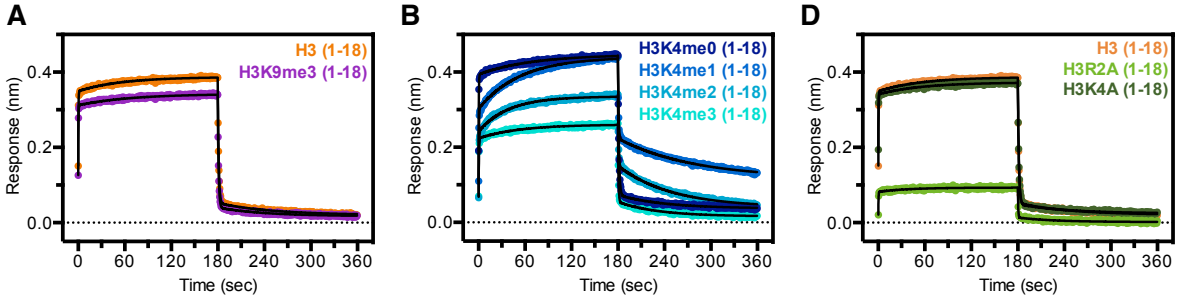

H3 (1-18) peptide	Association k_{obs1} (s^{-1})	Association k_{obs2} (s^{-1})	Dissociation k_{obs1} (s^{-1})	Dissociation k_{obs2} (s^{-1})
H3	3.23 ± 0.11	0.018 ± 0.001	0.87 ± 0.01	0.015 ± 0.001
H3K9me3	3.32 ± 0.18	0.015 ± 0.001	0.95 ± 0.01	0.016 ± 0.001

H3 (1-18) peptide	Association k_{obs1} (s^{-1})	Association k_{obs2} (s^{-1})	Dissociation k_{obs1} (s^{-1})	Dissociation k_{obs2} (s^{-1})
H3K4me0	3.07 ± 0.01	0.014 ± 0.0005	0.87 ± 0.01	0.017 ± 0.0007
H3K4me1	2.42 ± 0.02	0.018 ± 0.0003	1.34 ± 0.03	0.010 ± 0.0002
H3K4me2	2.02 ± 0.09	0.026 ± 0.0005	1.37 ± 0.04	0.014 ± 0.0003
H3K4me3	2.73 ± 0.11	0.019 ± 0.0008	1.55 ± 0.03	0.019 ± 0.0007

H3 (1-18) peptide	Association k_{obs1} (s^{-1})	Association k_{obs2} (s^{-1})	Dissociation k_{obs1} (s^{-1})	Dissociation k_{obs2} (s^{-1})
H3	3.23 ± 0.11	0.018 ± 0.0007	0.87 ± 0.01	0.015 ± 0.001
H3R2A	3.32 ± 0.36	0.025 ± 0.0026	2.09 ± 0.13	0.021 ± 0.002
H3K4A	3.61 ± 0.17	0.017 ± 0.0007	0.76 ± 0.01	0.016 ± 0.001

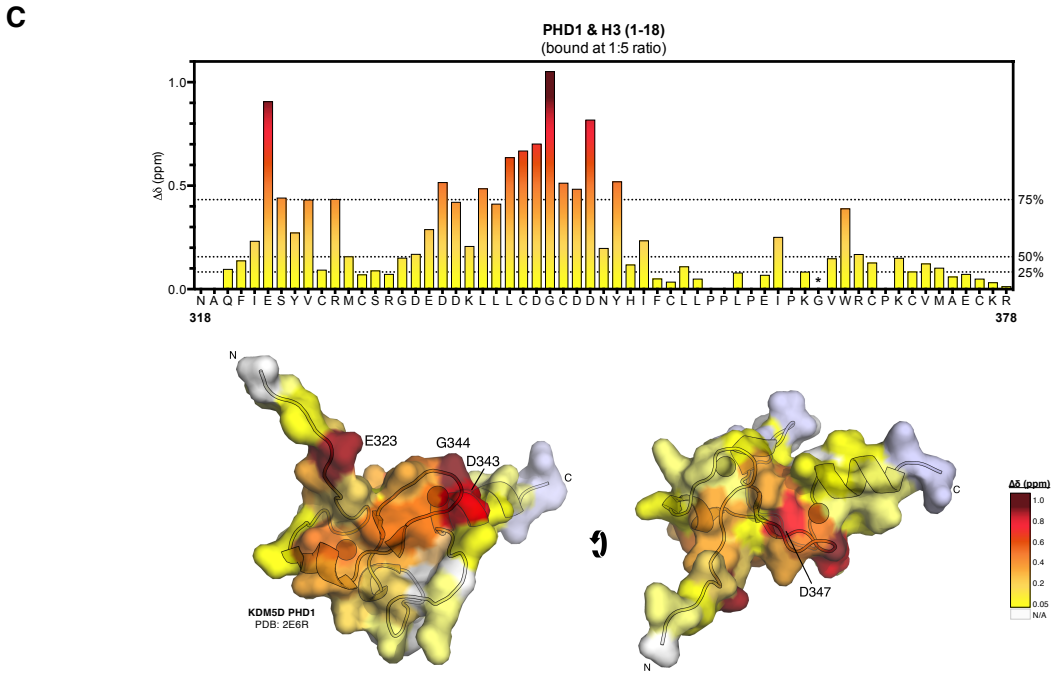

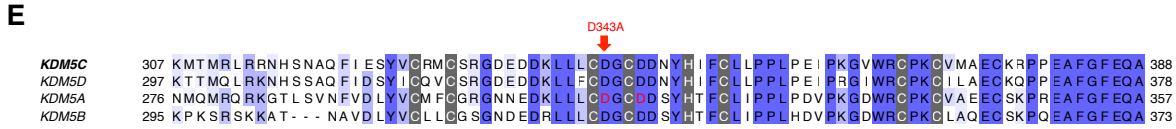

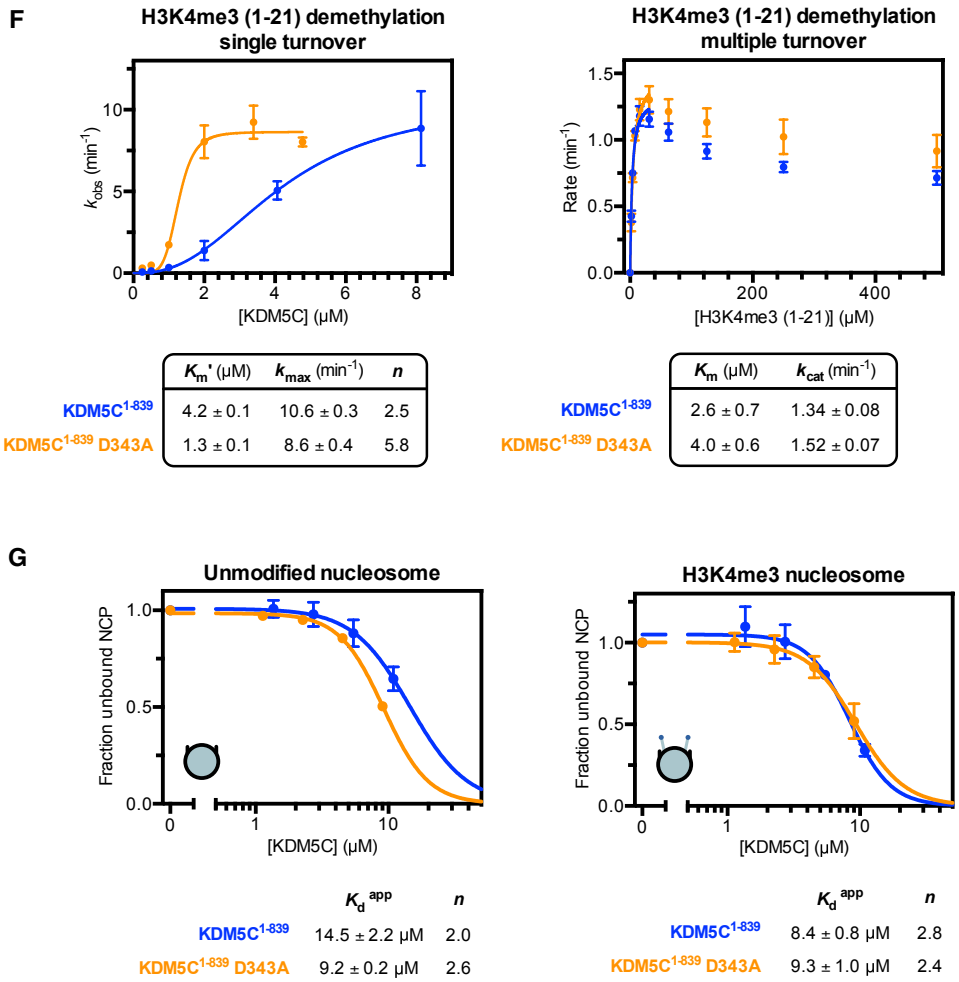

	K_m' (μM)	k_{max} (min^{-1})	n
KDM5C$^{1-839}$	4.2 ± 0.1	10.6 ± 0.3	2.5
KDM5C$^{1-839}$ D343A	1.3 ± 0.1	8.6 ± 0.4	5.8

	K_m (μM)	k_{cat} (min^{-1})
KDM5C$^{1-839}$	2.6 ± 0.7	1.34 ± 0.08
KDM5C$^{1-839}$ D343A	4.0 ± 0.6	1.52 ± 0.07

	K_d^{app}	n
KDM5C$^{1-839}$	14.5 ± 2.2 μM	2.0
KDM5C$^{1-839}$ D343A	9.2 ± 0.2 μM	2.6

	K_d^{app}	n
KDM5C$^{1-839}$	8.4 ± 0.8 μM	2.8
KDM5C$^{1-839}$ D343A	9.3 ± 1.0 μM	2.4

Figure S2. Related to Figure 2.
(A) Binding kinetic trace of immobilized Avitag-PHD1 binding to H3 (1-18) and H3K9me3 (1-18) tail peptides measured by bio-layer interferometry (BLI). Observed rates (k_{obs}) of association and dissociation are obtained by fitting kinetic traces to a two phase exponential function. **(B)** Binding kinetic trace of immobilized Avitag-PHD1 binding to H3K4me0/1/2/3 (1-18) tail peptides measured by bio-layer interferometry (BLI). Biphasic kinetic binding by PHD1 is modulated by the H3K4me state. **(C)** Chemical shift change of PHD1 residues upon binding of the H3 (1-18) tail peptide at 1:5 molar ratio (PHD:peptide) measured by NMR (*top*). The chemical shift change of G364 (* denoted by asterisk) could not be determined due to broadened chemical shift when bound. Dashed lines indicate 25th, 50th, and 75th percentile rankings, and residues are colored by a gradient from unperturbed (yellow) to significantly perturbed (maroon). Chemical shift perturbations colored by the gradient mapped to homologous residues in KDM5D PHD1 structure (PDB: 2E6R) (*bottom*). Significantly perturbed resides are labeled. **(D)** Binding kinetic trace of immobilized Avitag-PHD1 binding to H3 (1-18) and H3 mutant (1-18) tail peptides (H3R2A and H3K4A) measured by bio-layer interferometry (BLI). Recognition of the H3 tail by PHD1 depends on the R2 residue but not K4 residue in H3. **(E)** Sequence alignment of PHD1 domains in KDM5A-D. The H3R2 recognizing residues D312 and D315 of KDM5A are indicated in red, and the PHD1 mutation D343A from this study is denoted above KDM5C. Zinc coordinating residues are highlighted in gray. **(F)** H3K4me3 substrate peptide demethylation by PHD1 mutant KDM5C$^{1-839}$ relative to wild type. *Left*: Demethylation kinetics of the H3K4me3 (1-21) substrate peptide under single turnover conditions measured by a TR-FRET based kinetic assay. Observed rates are fit to a cooperative kinetic model, with *n* denoting the Hill coefficient. Unlike on the substrate nucleosome, the D343A PHD1 mutation does not increase catalytic rate on the substrate peptide, but does increase overall catalytic efficiency. *Right*: Demethylation kinetics of the H3K4me3 (1-21) substrate peptide under multiple turnover conditions measured by a formaldehyde release based kinetic assay. The D343A PHD1 mutation does not affect catalysis on the substrate peptide under these conditions, nor does it significantly affect substrate inhibition. **(G)** Unmodified and substrate core nucleosome binding by PHD1 mutant KDM5C$^{1-839}$ relative to wild type. Nucleosome binding curves were measured by EMSA and fit to a cooperative binding model to determine apparent dissociation constants (K_d^{app}), with *n* denoting the Hill coefficient. All error bars represent SEM of at least two independent experiments ($n \geq 2$).

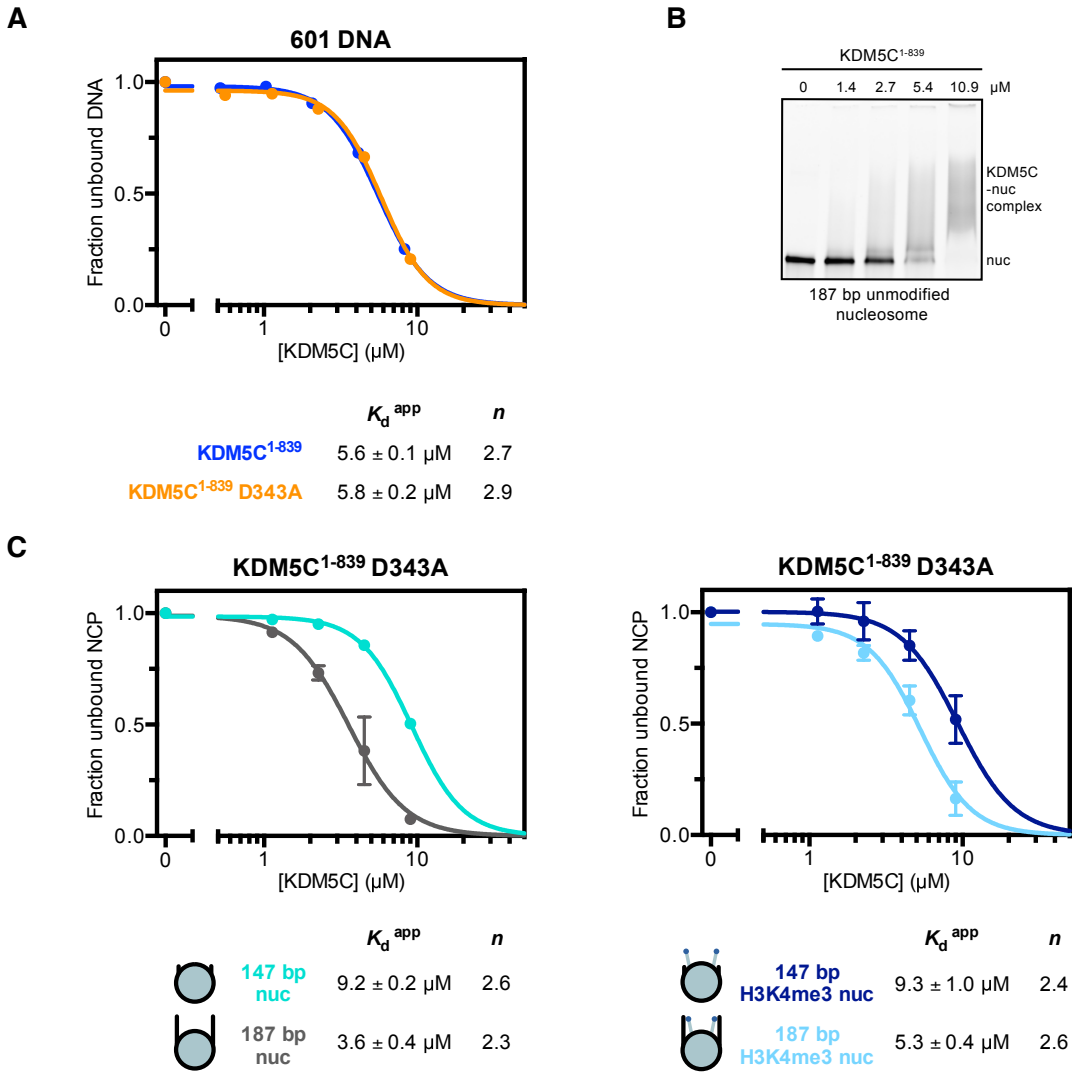

Figure S3. Related to Figure 3.
(A) Free DNA (147 bp 601 nucleosome positioning sequence) binding by KDM5C$^{1-839}$ and PHD1 mutant KDM5C$^{1-839}$. Binding curves were measured by EMSA and fit to a cooperative binding model to determine apparent dissociation constants (K_d^{app}), with n denoting the Hill coefficient. The D343A PHD1 mutation does not alter intrinsic DNA binding ability by KDM5C, indicating that PHD1 is not directly inhibiting the DNA binding surface of the ARID domain. **(B)** Representative gel shift of KDM5C$^{1-839}$ binding to the 187 bp nucleosome. **(C)** Binding curves of PHD1 mutant KDM5C$^{1-839}$ binding to unmodified and substrate nucleosomes with and without 20 bp flanking DNA. Nucleosome binding curves were measured by EMSA and fit to a cooperative binding model to determine apparent dissociation constants (K_d^{app}), with n denoting the Hill coefficient. All error bars represent SEM of at least two independent experiments ($n \geq 2$).

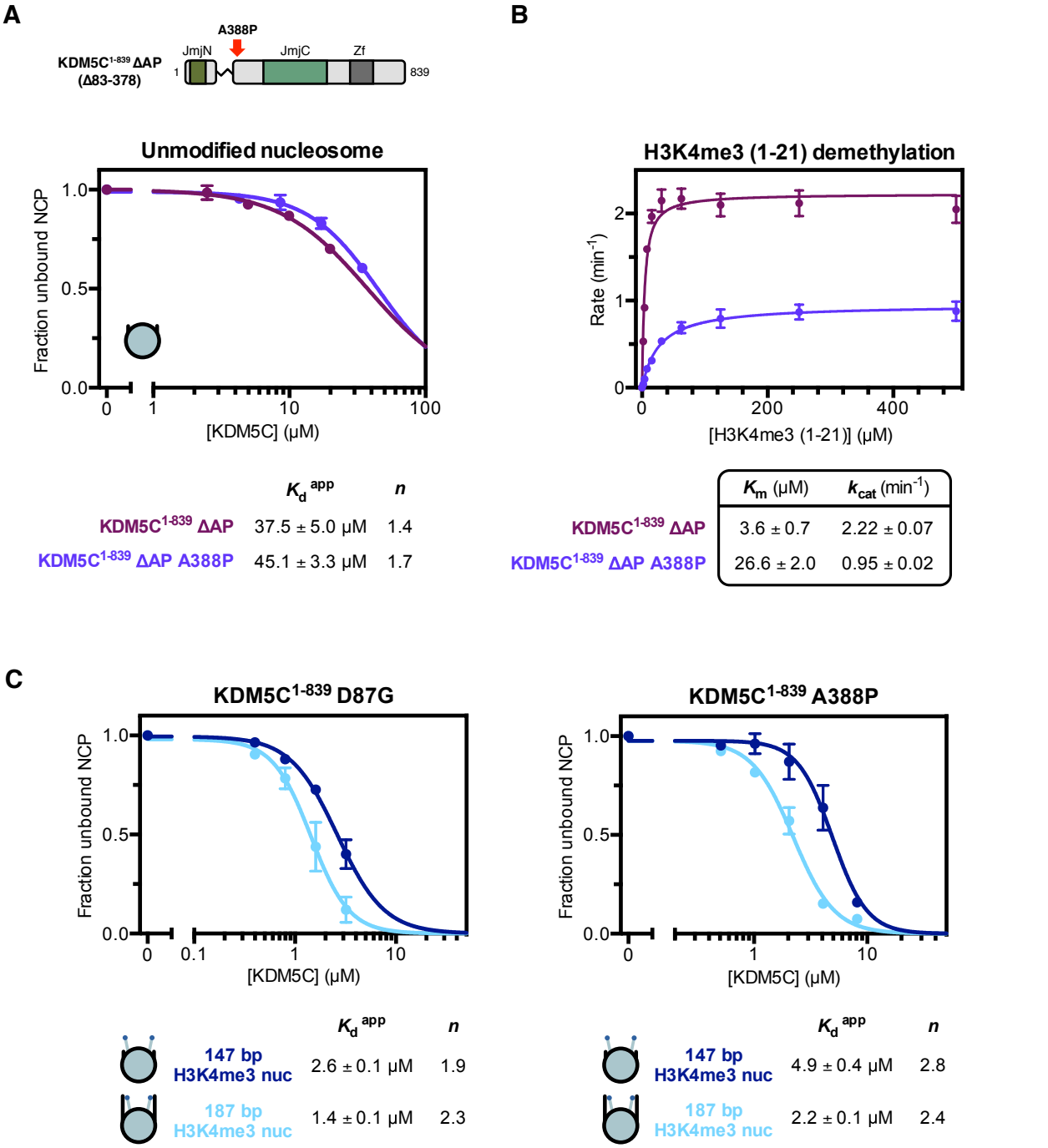

Figure S4. Related to Figure 5.
(A) Unmodified core nucleosome binding by KDM5C$^{1-839}$ ΔAP wild type and A388P. Nucleosome binding curves were measured by EMSA and fit to a cooperative binding model to determine apparent dissociation constants (K_d^{app}), with n denoting the Hill coefficient. The A388P mutation does not enhance nucleosome binding in the absence of the ARID and PHD1 region, indicating this region in KDM5C is altered by the A388P mutation to enable enhanced binding. **(B)** Demethylation kinetics of the H3K4me3 (1-21) substrate peptide by KDM5C$^{1-839}$ ΔAP wild type and A388P under multiple turnover conditions measured by a formaldehyde release based kinetic assay. The A388P mutation reduces demethylase activity of the catalytic domain alone, indicating distal structural disruption of the catalytic domain by this mutation. **(C)** Binding curves of KDM5C$^{1-839}$ D87G and A388P binding to substrate nucleosomes with and without 20 bp flanking DNA. All error bars represent SEM of at least two independent experiments ($n \geq 2$).

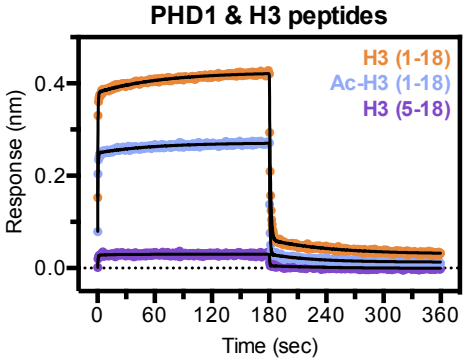

H3 peptide	Association		Dissociation	
	k_{obs1} (s^{-1})	k_{obs2} (s^{-1})	k_{obs1} (s^{-1})	k_{obs2} (s^{-1})
H3 (1-18)	2.79 ± 0.08	0.015 ± 0.0006	0.84 ± 0.01	0.015 ± 0.0009
Ac-H3 (1-18)	2.51 ± 0.08	0.016 ± 0.0011	1.63 ± 0.03	0.022 ± 0.0016
H3 (5-18)	2.14 ± 0.26	0.063 ± 0.0217	2.34 ± 0.48	0.015 ± 0.0040

Figure S5. Related to Discussion.
Binding kinetic trace of immobilized Avitag-PHD1 binding to H3 (1-18), N-terminally acetylated H3 (1-18), and H3 (5-18) tail peptides measured by bio-layer interferometry (BLI). Observed rates (k_{obs}) of association and dissociation are obtained by fitting kinetic traces to a two phase exponential function. Recognition of the H3 tail by PHD1 does not strongly depend on the H3 N-terminus but does depend on the first 4 residues of H3 (ARTK).

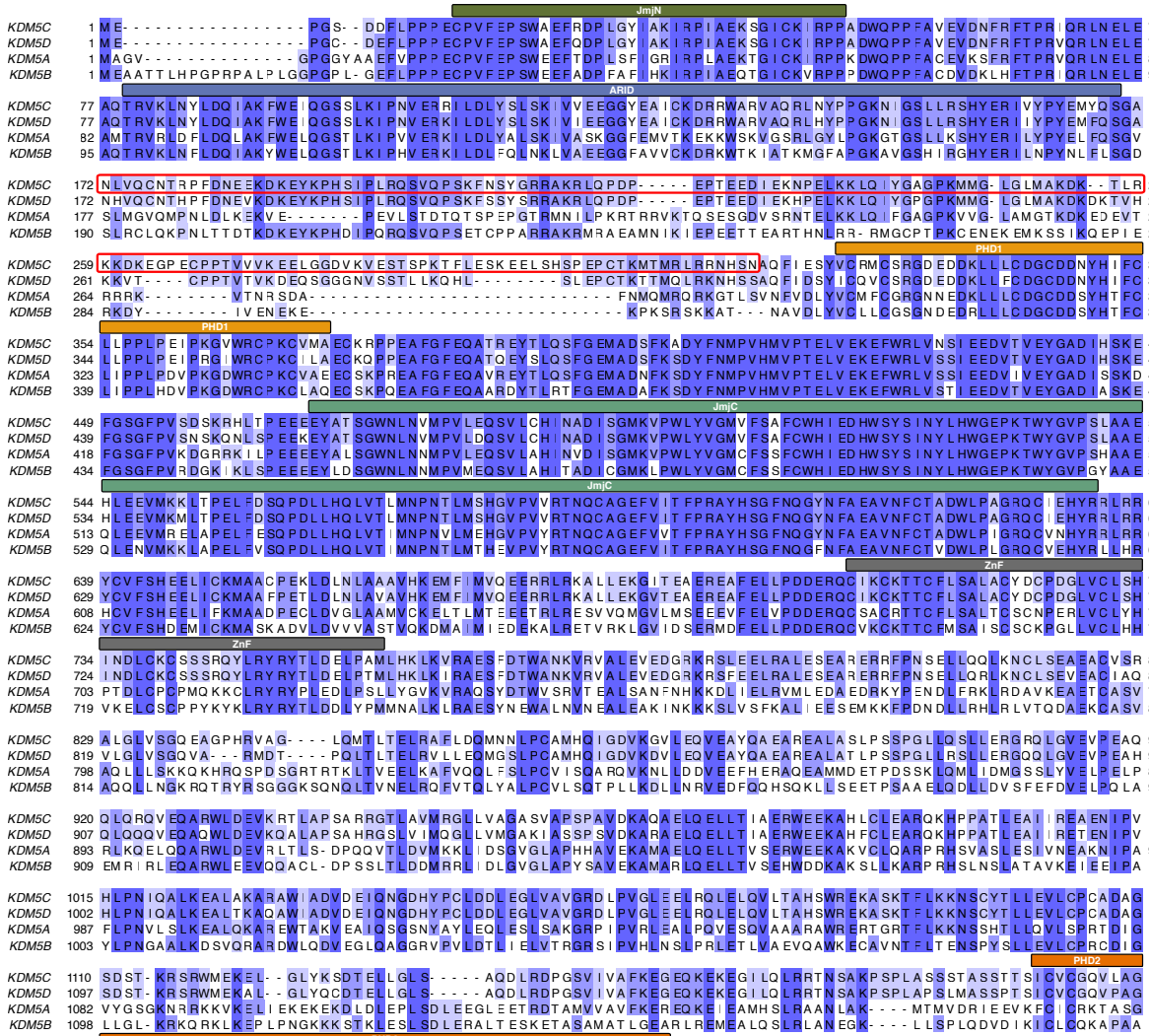

Figure S6. Related to Discussion.
Sequence alignment of human KDM5A-D with annotated domains. KDM5C has a different and extended linker region between ARID and PHD1 (boxed in red).